Segmentation of AFM-Images Based on Wave Region Growing of Local Maxima

Oday Jasim Mohammed Al-Furaiji, Violetta Viktorovna Rabtsevich, Viktar Yurevich Tsviatkou, Tatiana Anatolyevna Kuznetsova, and Sergey Antonovich Chizhik

***Abstract*—In this paper, a segmentation algorithm for atomic force microscopy images has been developed, using wave region growing around local maxima as a result of joining adjacent pixels to the regions, which are selected in decreasing order of values. The essence of the algorithm consists in using the brightness threshold, which is gradually changing from maximum to minimum, in order to select growing points or to join existing areas. The iteratively expandable boundaries, and the choice of initial growing points and points that are attached to areas with a focus on threshold values with a gradual decrease from maximum to minimum, are considered features of the developed segmentation algorithm. These features made it possible to eliminate errors of marker watershed, region growing algorithms and watershed using the classical Vincent-Sollie algorithm, which are usually used in segmentation of AFM-images. The developed algorithm is compared with the following standard algorithms: classic watershed algorithm, marker watershed, region growing. The comparison is made on test and original AFM-images. The algorithms are implemented in Matlab and C ++. To quantify segmentation errors, a set of binary masks is used. The experiments showed that the developed algorithm selects the region boundaries without errors and with higher segmentation speed in comparison with the algorithms for region growing and Vincent – Sollie watershed.**

***Index Terms*—image segmentation, atomic force microscopy, region growing, Vincent–Sollie watershed, local maximum, AFM-images, marker watershed**

I. Introduction

The structural components size determination is considered one of the key tasks of materials science in identifying the relationship «structure-properties» [1–3]. Atomic force microscopy (AFM) is often considered as the most informative method for studying the surface and the results of its modification in the submicro- and nanoscale range [4–6]. When determining the structural components size in the automatic mode, the segmentation of AFM-images is considered as one of the problems, which allows one particle, phase or grain to be separated from another [7, 8]. The problem lies in the specifics of AFM-images, where the brightness of pixels carries information about the surface relief or the intensity of the force action from the surface on the microprobe [9–11]. The segmentation in conditions, when the brightness of boundaries does not have significant contrast with separated objects and the merged objects, is particularly difficult [12–15]. Threshold segmentation algorithms [16] that are often used in AFM have minimal computational complexity, but allow obtaining correct results only in the case of a simple topology of the surface, which is divided into objects and a background, when the choice of the threshold does not affect the number of allocated segments. For segmentation of images with complex topology, as a rule, algorithms for region growing [17] are used, which have relatively low computational complexity, as well as more complex algorithms of morphological watershed (using a gradient and marker [18]). In the algorithms of region growing, the initial points of growth are selected, to which adjacent pixels with similar brightness are attached. Gradient watershed algorithms (Beucher [19], Vincent-Sollie [20], Jackway [21], Weickert [22], Young-Scharcanski [23]) use the gradient calculation for each pixel in the image, the determination of local minima, and pixel bypass depending on priority (priority is determined by the brightness of pixels). Marker watershed algorithms use morphological open and close operations to automatically place markers of the background and objects. When processing AFM-images with a complex topology using algorithms for region growing [17], insufficient or excessive segmentation is often manifested due to errors in determining the initial points of region growing, inaccuracy in setting criteria for completing their growth process, and incorrect sequence of processing regions. Similar errors in the conditions under consideration are typical for gradient and marker watershed algorithms with automatic marker placement [19–23], which do not fully take into account the specifics of AFM-images in which the pixel brightness is directly related to the values of physical parameters, which leads to errors in determining the watershed lines and marker locations. The watershed algorithms under operator control [24] can significantly reduce or completely eliminate segmentation errors due to the placement of markers by the operator, but they require significant time and are therefore

Manuscript received October 14, 2019; revised February 05, 2020.

Oday Jasim Mohammed Al-Furaiji was with Belarusian State University of Informatics and Radioelectronics, Minsk, Belarus. He is now with the Department of Computer Science, Shatt Al-Arab University College, Basra, Iraq (e-mail: odaymohammed@mail.ru).

Violetta Viktorovna Rabtsevich is with Belarusian State University of Informatics and Radioelectronics, Minsk, Belarus (e-mail: rabcevichv@gmail.com).

Viktar Yurevich Tsviatkou is with Belarusian State University of Informatics and Radioelectronics, Minsk, Belarus (e-mail: vtsvet@bsuir.by).

Tatiana Anatolyevna Kuznetsova is with A.V. Luikov Heat and Mass Transfer Institute of the National Academy of Sciences, Minsk, Belarus (e-mail: kuzn06@mail.ru).

Sergey Antonovich Chizhik is with A.V. Luikov Heat and Mass Transfer Institute of the National Academy of Sciences, Minsk, Belarus (e-mail: chizhik_sa@tut.by).

effective for processing AFM-images of surfaces with only a small number of objects. To eliminate these drawbacks, it is proposed to associate the processes of selecting the starting points and the growth of regions with a value change in the brightness threshold of the pixels of the AFM-image from maximum to minimum. This will provide automatic selection and ordering of the initial growth points by brightness, the same growth rate of regions regardless of their location, size and shape, but taking into account their brightness, uniform division of the entire image into regions (full segmentation).

II. Algorithm of Wave Region Growing of Local Maxima

A segmentation algorithm of AFM-images based on wave region growing of local maxima with a selection of pixels in a decreasing order of values (RGLM) is proposed. The essence of the algorithm is to use the brightness threshold, which varies from maximum to minimum, to select pixels of AFM-images that form growth points of regions (local maxima) or join existing regions (adjacent to pixels included in regions and having the same or higher brightness). In contrast to the classical region growing [18], which uses sequential processing of segments, in the proposed algorithm, the boundaries of all regions expand iteratively (wave-like) due to attaching unprocessed adjacent significant pixels, the brightness of which satisfies the threshold lowered after processing all significant pixels. In contrast to tree-wave region growing [25], which determines all growth points during initialization and attaches adjacent pixels to regions without taking their values into account, in the proposed algorithm, the choice of initial growth points and adjoining regions of adjacent pixels is associated with a threshold value that is gradually reduced from maximum to a minimum.

The RGLM algorithm for wave region growing of local maxima consists of the following steps.

1) Loading the scan matrix $M_Z = \left\| m_Z\left(y,x\right)\right\|_{\left(y=\overline{0,Y-1},x=\overline{0,X-1}\right)}$, in which the value of each B-bit element $m_Z\left(y,x\right)\in\left[0,2^B-1\right]$ is determined by the height (friction or viscosity) corresponding to the surface point, where Y, X – are the dimensions of scan matrix vertically and horizontally.

2) Forming the segmentation matrix $M_S = \left\| m_S\left(y,x\right)\right\|_{\left(y=\overline{0,Y-1},x=\overline{0,X-1}\right)}$, the elements of which are determined using the expression $m_S\left(y,x\right)\leftarrow 0$, at $y=\overline{0,Y-1}$, $x=\overline{0,X-1}$. The segment counter C_S is set to zero: $C_S\leftarrow 0$.

3) The segmentation cycle counter C_Q is assigned the brightness threshold value, corresponding to the upper quantization level of pixel values of the AFM-image: $C_Q\leftarrow 2^B-1$.

4) Beginning of the segmentation cycle.

Forming the significance matrix $M_Q\left(C_Q\right)=\left\| m_Q\left(C_Q,y,x\right)\right\|_{\left(y=\overline{0,Y-1},x=\overline{0,X-1}\right)}$ for the brightness threshold value C_Q, the elements of which are determined using the expression

$$\begin{cases}\left(m_Z\left(y,x\right)=C_Q\right)\Rightarrow\left(m_Q\left(C_Q,y,x\right)\leftarrow 1\right),\\ \left(m_Z\left(y,x\right)\neq C_Q\right)\Rightarrow\left(m_Q\left(C_Q,y,x\right)\leftarrow 0\right)\end{cases} \tag{1}$$

at $y=\overline{0,Y-1}$, $x=\overline{0,X-1}$.

5) Checking the significance matrix to zero. The sum of all elements of the significance matrix $M_Q\left(C_Q\right)$ for the brightness threshold value C_Q is calculated using the expression

$$S_Q=\sum_{y=0}^{Y-1}\sum_{x=0}^{X-1}m_Q\left(C_Q,y,x\right). \tag{2}$$

If $S_Q=0$, then go to the end of the segmentation cycle (step 15).

6) Checking the segment counter to zero. If $C_S=0$, then go to step 13 to search for new regions.

7) The wave segmentation cycle counter C_W is set to zero: $C_W\leftarrow 0$.

8) Beginning of the wave segmentation cycle.

Forming the region growing matrix $M_T\left(C_Q,C_W\right)=\left\| m_T\left(C_Q,C_W,y,x\right)\right\|_{\left(y=\overline{0,Y-1},x=\overline{0,X-1}\right)}$ for the brightness threshold value C_Q and C_W-th segmentation level, the elements of which are determined using the expression $m_T\left(C_Q,C_W,y,x\right)\leftarrow 0$ at $y=\overline{0,Y-1}$, $x=\overline{0,X-1}$.

9) Wave region growing. The matrix elements $M_T\left(C_Q,C_W\right)$ are redefined using the expression

$$\begin{gathered}\left(m_S\left(y,x\right)\neq 0\right)\wedge\left(m_Q\left(C_Q,y+j,x+i\right)=1\right)\wedge\\ \left(m_T\left(C_Q,C_W,y+j,x+i\right)=0\right)\Rightarrow\left(m_T\left(C_Q,C_W,y+j,x+i\right)\leftarrow m_S\left(y,x\right)\right)\end{gathered} \tag{3}$$

at $y=\overline{0,Y-1}$, $x=\overline{0,X-1}$, $j=\overline{-1,1}$, $i=\overline{-1,1}$.

10) Checking the exit condition from the wave region growing cycle. The number of significant elements S_T of the matrix $M_T\left(C_Q,C_W\right)$ is determined using the expression

$$S_T=\sum_{y=0}^{Y-1}\sum_{x=0}^{X-1}m_T\left(C_Q,C_W,y,x\right) \tag{4}$$

at $y=\overline{0,Y-1}$, $x=\overline{0,X-1}$.

If $S_T=0$ (there are no new connected elements), then exit the wave segmentation cycle and go to step 13. The value of the wave segmentation cycle counter C_W indicates the number of growth orbits.

11) Updating the segmentation matrix. New significant elements are added to the segmentation matrix M_S using the expression

$$m_S\left(y,x\right)\leftarrow m_S\left(y,x\right)+m_T\left(C_Q,C_W,y,x\right) \tag{5}$$

at $y=\overline{0,Y-1}$, $x=\overline{0,X-1}$.

12) Ending the wave segmentation cycle. The value of the

wave segmentation cycle counter C_W is increased by one: $C_W \leftarrow C_W + 1$ and go to the beginning of the wave segmentation cycle at step 8.

13) Searching for new regions. The matrix elements $M_Q\left(C_Q\right)$ satisfying the condition, are segmented using the region growing algorithm [17]. As a result, a matrix $M_N\left(C_Q\right) = \left\| m_N\left(C_Q, y, x\right)\right\|_{\left(y=\overline{0,Y-1}, x=\overline{0,X-1}\right)}$ of new regions is formed for the brightness threshold value C_Q, the element numbers $m_N\left(C_Q, y, x\right) \in \left[1, C_N\left(C_Q\right)\right]$ of which, indicate isolated sets of individual elements of the matrix $M_Q\left(C_Q\right)$, that satisfy condition (1), where $C_N\left(C_Q\right)$ – is the number of segments selected in the matrix $M_Q\left(C_Q\right)$.

14) Addition of the segmentation matrix with new regions. The numbers are transferred from the matrix $M_N\left(C_Q\right)$ of new regions to the segmentation matrix M_S and increment the segment counter using the expressions

$$\left(m_N\left(C_Q, y, x\right) > 0\right) \Rightarrow \left(m_S\left(y, x\right) \Leftarrow m_N\left(C_Q, y, x\right) + C_S\right) \quad (7)$$

at $y = \overline{0, Y-1}$, $x = \overline{0, X-1}$,

$$C_S = C_S + C_N\left(C_Q\right). \quad (8)$$

15) Ending the segmentation cycle. The value of the segmentation cycle counter C_Q is decreased by one: $C_Q \leftarrow C_Q - 1$, which corresponds to a decrease by one unit of the brightness threshold value. Then the cycle counter C_Q is checked for a negative value. If $C_Q \geq 0$, then go to the beginning of the segmentation cycle (step 4 of the algorithm). If $C_Q < 0$, then exit cycle and end the algorithm.

As a result of implementing this algorithm a segmentation matrix M_S is formed, the element numbers of which $m_N\left(C_Q, y, x\right) \in \left[1, C_N\left(C_Q\right)\right]$ at $y = \overline{0, Y-1}$, $x = \overline{0, X-1}$ indicate the segments to which they belong.

III. Evaluation of AFM-Image Segmentation Results

To objectively evaluate the segmentation results of AFM-images, a set $\left\{M_T\left(j\right)\right\}_{\left(j=\overline{1,J}\right)}$ of J =6 test AFM-matrices $M_T\left(j\right) = \left\| m_T\left(j, y, x\right)\right\|_{\left(y=\overline{0,Y-1}, x=\overline{0,X-1}\right)}$ of size $Y \times X$ vertically and horizontally is formed, the elements $m_T\left(j, y, x\right)$ of which contain information about the distances from the substrate to the surfaces of the test objects of the same size located on it. The bases of these objects lie in parallel planes, and the projections of their central points on the substrate are in the nodes of the virtual square grid. The first AFM-matrix sets the location of 9 hemispheres of the same height; the second – 9 fragments of spheres of various heights; the third – 9 tori of the same height; the fourth and fifth – 9 tori and pyramids from fragments of spheres; the sixth – combinations of 18 fragments of spheres. Fig. 1 shows test AFM-images obtained by converting the value of each element of the AFM-matrix into the brightness of the corresponding pixel. For each test AFM-image is shown in Fig. 2 by three horizontal brightness profiles. The profiles are obtained along straight lines passing through the centers of horizontal projections of test objects. The result of incomplete segmentation of test AFM-images with interruption of processing at the substrate level should be a matrix in which the elements corresponding to the surfaces of the test objects take values of segment numbers (from 1 to 9 for the test AFM-images shown in Fig. 1,a–e; from 1 to 18 for the test AFM-image shown in Fig. 1,f), and the elements corresponding to the space between the test objects (substrate) take zero values (reference matrix of incomplete segmentation). The result of complete segmentation of the test AFM-images should be a matrix in which the elements corresponding to the surfaces of the test objects and adjacent fragments of the substrate take the values of the segment numbers (from 1 to 9 for the test AFM-images shown in Fig. 1,a–e; from 1 to 18 for the test AFM-image shown in Fig. 1,f) (reference matrix of complete segmentation).

To evaluate segmentation errors, a set of binary masks is used (Fig. 3). Three masks represent the projections of test objects on a substrate, which are formed as a result of binarization of the reference segmentation matrices, and are designed to evaluate errors of incomplete segmentation. Two masks are formed as a result of dividing the reference segmentation matrix into 9 squares of the same size (for AFM-images, shown in Fig. 1,a–e) and 18 rectangles (for the AFM-image, shown in Fig. 1,f). They are designed to evaluate the complete segmentation errors. The segmentation matrices obtained by various algorithms are compared with the masks, and the normalized segmentation error E_S is calculated using the expression

$$E_S = E_O + E_I,$$

where $E_O = \dfrac{\sum_{i=1}^{9} S_O\left(i\right)}{S_E}$ – is the normalized error of excessive segmentation; $E_I = \dfrac{\sum_{i=1}^{9} S_I\left(i\right)}{S_E}$ – is the normalized error of incomplete segmentation; i – is the serial number of the test object; S_E – is the number of significant mask elements; $S_O\left(i\right)$ – is the number of pixels, of the segment corresponding to the i-th test object, that fall into insignificant elements of the mask; $S_I\left(i\right)$ – is the number of significant mask elements corresponding to the i-th test object that do not fall into the pixels of the corresponding segment.

For a mask corresponding to test AFM-images of fragments of spheres (Fig. 1,a–e), the S_E value is calculated using the expression $S_E = \lceil 2\pi R_E i \rceil$, where R_E – is the largest radius of a fragment of a sphere or torus (in pixels) at the substrate level; $\lceil\ \rceil$ – is the excess rounding operation to the nearest integer.

Figures 4–11 show the images of segmentation matrices of 6 test AFM-images (the values of the elements of the segmentation matrices are converted to the brightness of the corresponding pixels).

Figures 4 and 5 show incomplete and complete

segmentation using the proposed RGLM algorithm (implementations in the Matlab environment and in the C ++ programming language using the OpenCV library); Fig. 6 shows incomplete segmentation using the MWA algorithm of the marker watershed with automatic placement of foreground and background markers based on the gradient, morphological opening and closing operations (implementation in Matlab) [10]; Fig. 7 shows incomplete segmentation using the MWUC algorithm of the marker watershed under the control of the operator (implementation in C ++) [16]; Fig. 8 shows incomplete segmentation using the RG algorithm for region growing with the selection of starting points based on the histogram (implementation in Matlab) [17]; Fig. 9 shows incomplete segmentation using the RG algorithm (implementation in C ++); Fig. 10 shows incomplete segmentation using the Vincent-Sollie VSG algorithm with preliminary calculation of the gradient in an eight-connected area (implementation in Matlab) [18]; Fig. 11 shows segmentation using the Vincent-Sollie VSC algorithm with the allocation of the contours of the regions and their subsequent filling (implementation in C ++) [19].

For the investigated algorithms [26–29], the values of normalized errors E_S, E_O and E_I of incomplete segmentation are given in Table I, and the processing time is shown in Table II. Table I shows, that the proposed RGLM algorithm provides incomplete segmentation without errors. Other algorithms segment all test AFM-images with errors. Implementation of the VSC algorithm does not allow the segmentation of AFM-1, AFM-2 and AFM-6. Errors of complete segmentation of AFM-images using the proposed algorithm appear only on AFM-6 (error value 0.6). Other investigated algorithms do not provide complete segmentation of AFM-images.

Table I shows that, some test AFM-images are segmented with a relatively small error by MWUC algorithm of a marker watershed under the operator control. Segmentation errors using MWUC, strongly depend on the accuracy of marker placement by the operator (Fig. 12). However, this operation requires significant time costs, especially with a large number of segments. In the MWA algorithm of a marker watershed with automatic marker placement, the background and object markers are determined based on the gradient, which leads to a sharp increase in segmentation error (by 3 – 30 times depending on the type of image).

The obtained segmentation results of test AFM-images are compared with the results of the Gwyddion program [30] (Fig. 13), which uses the Vincent-Sollie algorithm. Using this program, incomplete segmentation of AFM-images can be implemented without errors, however, this requires the use of additional blur, calculation and estimation of the gradient, preliminary inversion of the brightness values, filling of the contoured fragments. These operations are carried out under the control of the operator. In addition, the obtained results are represented in a binary matrix in which unit elements correspond to object pixels, which additionally requires brightness segmentation to determine the number for each segment. Additional operations and operator involvement lead to significant time costs.

Table II shows that, when the proposed algorithm is implemented in Matlab, it provides an average of 53 times lower operating speed compared to the marker watershed, and 10 times higher operating speed compared to the algorithms of region growing and watershed of Vincent-Sollie. Also, when the proposed algorithm is implemented in C ++, it provides an average of 1.3 times lower operating speed compared to a marker watershed, 1.4 and 1.6 times higher operating speed compared to region growing and the watershed using Vincent-Sollie algorithm, respectively (taking into account the time spent on marker placement by the operator and using additional segmentation algorithms to determine segment numbers).

The proposed algorithm of region growing is compared with algorithms implemented in the Matlab environment: marker watershed with automatic marker placement MWA, region growing RG. To implement the evaluation, a database of test images was created in the Gwyddion environment (for evaluating homogeneity and contrast), which were divided into two large categories: images of the first type (Fig. 14 a, b; Fig. 15), having detached elements on the substrate and of the second type (Fig. 14 c, d, Fig. 16.), having coalesced groups of elements on the substrate. To implement these types of images in Gwyddion using the “synthesize” tool, 205 test images were created with objects of different properties and sizes (Table III).

As can be seen from Table III, eight types of images synthesized in Gwyddion were selected for this experiment. Each of them contains objects of various sizes, features and relative positions [19]. The main types of test images are shown in (Fig. 14-16). Segmentation results are presented in (Fig. 17-22).

Evaluation of the work (Table IV) of the selected algorithms was implemented by the number of segments, by the contrast between segments, by the homogeneity of the segments.

To evaluate the performance of the presented algorithms, we compare the results of their work on the original AFM-images, to which the algorithms of brightness equalization and filtering are applied (Fig. 23–26).

As can be seen from the data presented, the RGLM algorithm is better suited for images of the second type, it allows to find borders between two segments, even if they are at different heights and the transition between them is blurred. Two types of watershed algorithms show either excessive or insufficient segmentation on two types of images. On all types, the algorithm of region growing shows excessive segmentation. The current algorithm requires preliminary processing of AFM-images to correctly display the number of segments.

Obviously, from (Fig. 23–26), the watershed method using the classical Vincent-Sollie algorithm leads to the appearance of superfluous segments, especially in images with fuzzy borders. The method of morphological marker watershed without operator participation in turn leads to insufficient image segmentation, many segments are lost. The developed RGLM algorithm makes it possible to split the original image into segments, however it is sensitive to artifacts in the image, which can lead to false segments in the image.

Table V shows that, by the homogeneity of brightness within each segment, all models, except for MWA, show a consistently high result. The number of segments within an

image is insufficient for further analysis by the RG and MWA models. The highest contrast value between adjacent segments is shown by the RG algorithm, however, due to the minimum number of segments, this indicator does not fully reflect the quality of segmentation. A complex criterion that takes into account not only the number of segments, but also their quality in such indicators as the segment homogeneity, its area and fine for the large number of small segments, shows the best result for the RGLM model.

IV. Conclusion

In this paper, an algorithm for segmenting AFM-images based on wave region growing of local maximum with a choice of pixels in decreasing order of values has been developed. The essence of the algorithm is to use the brightness threshold, which varies from maximum to minimum, to select AFM-image pixels that form growing points of regions (local maxima) or join existing regions (adjacent to pixels included in regions and having the same or higher brightness). This allowed to eliminate segmentation errors of AFM-images, that are characteristic for the algorithms of marker watershed (with automatic and manual marker placement), region growing, and the Vincent-Sollie watershed. In comparison with the algorithms of region growing and Vincent-Sollie watershed, the developed algorithm provides an increase in segmentation speed by 1.4 and 1.7 times, respectively, when implemented in the C ++ programming language.

TABLE I
Values of Normalized Segmentation Errors of Test AFM-Images

Images	Errors	Values of normalized segmentation errors ($\times 10^{-3}$) for algorithms:							
		Implementation in Matlab				Implementation in C++			
		RGLM	MWA	RG	VSG	RGLM	MWUC	RG	VSC
AFM-1	E_O	0	0	0	0	0	10.172	0	–
	E_I	0	39.888	46.316	34.998	0	0	55.171	–
	E_S	0	39.888	46.316	34.998	0	10.172	55.171	–
AFM-2	E_O	0	0	0	0	0	10.172	0	–
	E_I	0	39.888	41.192	35.015	0	0	55.171	–
	E_S	0	39.888	41.192	35.015	0	10.172	55.171	–
AFM-3	E_O	0	109.590	98.626	109.590	0	94.643	109.590	0.110
	E_I	0	44.260	52.043	46.125	0	0.528	81.736	0.615
	E_S	0	153.849	150.668	155.715	0	95.171	191.326	0.725
AFM-4	E_O	0	0	0	41.570	0	10.172	0	0.463
	E_I	0	41.213	72.369	0	0	0	73.664	517.115
	E_S	0	41.213	72.369	41.570	0	10.172	73.664	517.577
AFM-5	E_O	0	0	0	43.709	0	10.172	0	0.475
	E_I	0	359.926	56.475	0	0	0	79.930	523.079
	E_S	0	359.926	56.475	43.709	0	10.172	79.930	523.555
AFM-6	E_O	0	0	42.151	73.579	0	19.853	0	2034.901
	E_I	0	17.948	78.292	0	0	0	96.055	0
	E_S	0	17.948	78.334	73.579	0	19.853	96.055	2034.901

TABLE II
Incomplete Segmentation Time for Test AFM-Images

Images	Values of incomplete segmentation time (ms) for the algorithms:							
	Implementation in Matlab				Implementation in C++			
	RGLM	MWA	RG	VSG	RGLM	MWUC	RG	VSC
AFM-1	27297.358	561.433	249176.870	249177	6378.000	4791	8470.000	9759
AFM-2	21006.743	533.003	244676.704	244677	5716.000	4790	7756.000	9248
AFM-3	23117.077	442.969	287707.800	287708	5957.000	4794	8196.000	9848
AFM-4	29948.149	491.136	281089.985	281091	7674.000	9292	9781.000	9594
AFM-5	30288.289	454.526	295065.221	295066	7824.000	13797	9907.000	11251
AFM-6	26438.857	492.037	250362.477	250363	3907.000	9302	6988.000	8368
Average for AFM-1 – AFM-6	26349.410	495.851	268013.200	267680.300	6242.667	8394.219	8516.333	9678.000

TABLE III
TYPES OF TEST IMAGES SYNTHESIZED USING THE GWYDDION PROGRAM

First type		Second type	
Numbers of tests images	Type of test images	Numbers of tests images	Type of test images
AFM_G1 -1 – AFM_G1-26	«hemispheres»	AFM_G2 -1 – AFM_G2 -20	«hemispheres»
AFM_G1 -27 – AFM_G1 -45	«bagels»	AFM_G2 -21 – AFM_G2 -35	«bagels»
AFM_G1 -46 – AFM_G1 -55	«half weld point»	AFM_G2 -36 – AFM_G2 -45	«half weld point»
AFM_G1 -56 – AFM_G1 -65	«weld point»	AFM_G2 -46 – AFM_G2 -55	«weld point»
AFM_G1 -66 – AFM_G1 -80	«full spheres»	AFM_G2 -56 – AFM_G2 -61	«full spheres»
AFM_G1 -81 – AFM_G1 -90	«donuts»	AFM_G2 - 62 – AFM_G2 -71	«donuts»
AFM_G1 -91 – AFM_G1 -100	«ellipsoids»	AFM_G2 -72 – AFM_G2 -76	«ellipsoids»
AFM_G1 -100 – AFM_G1-105	«disks»	AFM_G2 -77 – AFM_G2 -80	«fiber»
		AFM_G2 -81 – AFM_G2 -94	«disks»
		AFM_G2 -95 – AFM_G2 -100	«domains»

TABLE IV
THE OPERATION RESULTS OF THE SELECTED ALGORITHMS BASED ON THE GRAYSCALE IMAGES DATABASE PRESENTED ABOVE

Criteria	First type of images			Second type of images		
	RGLM	MWA	RG	RGLM	MWA	RG
	Number of segments			Number of segments		
Average error (segment)	1.0333	522.0556	10943.9800	80.7000	421.5780	63748
	Segment homogeneity			Segment homogeneity		
Values range (min – max)	0,6418-0,9888	0,8641-1,0000	1,0000-10000	0,6386-0,9861	0,7367-0,9819	1,0000-1,0000
Average value	0,7549	0,9353	1,0000	0,8108	0,9040	1,0000
	Contrast between segments			Contrast between segments		
Values range (min – max)	0,0742-0,04378	0,7776-1,0000	0,0000-0,0000	0,0532-0,3284	0,0152-0,9907	0,0000-0,0000
Average value	0,14383	0,9563	0,0000	0,1615	0,6612	0,0000

TABLE V
THE OPERATION RESULTS OF THE SELECTED ALGORITHMS BASED ON THE GRAYSCALE IMAGES DATABASE PRESENTED ABOVE

Segmentation algorithm	Evaluation measure	Test-1	Test-2	Test-3	Test-4	Test-5	Test-6	Average value
RGLM	Segment homogeneity	0.9660	0.9449	0.9678	0.9628	0.9630	0.9641	0.9614
	Number of segments	1116	602	689	122	125	820	579
	Contrast between segments	0.3401	0.3897	0.3357	0.4045	0.4007	0.3569	0.3713
	Complex criteria (10^{-6})	1.1173	1.047	0.0938	0.0484	0.0559	0.1581	0.4201
RG	Segment homogeneity	0.9245	0.9640	0.8677	0.9532	0.9633	0.9583	0.9385
	Number of segments	163	82	55	29	55	56	73
	Contrast between segments	0.3923	0.3629	0.3234	0.4543	0.3473	0.4813	0.3936
	Complex criteria (10^{-6})	2.4726	0.0786	12.0740	0.0139	0.0271	0.1216	2.4646
MWA	Segment homogeneity	0.9275	0.9894	0.8984	0.9302	0.9364	0.8781	0.9267
	Number of segments	18	7	27	29	29	11	20
	Contrast between segments	0.3420	0.1742	0.3156	0.3631	0.4061	0.2269	0.3047
	Complex criteria (10^{-6})	0.4518	4.4633×10^{-5}	0.7769	0.2820	0.2983	1.9520	0.6268

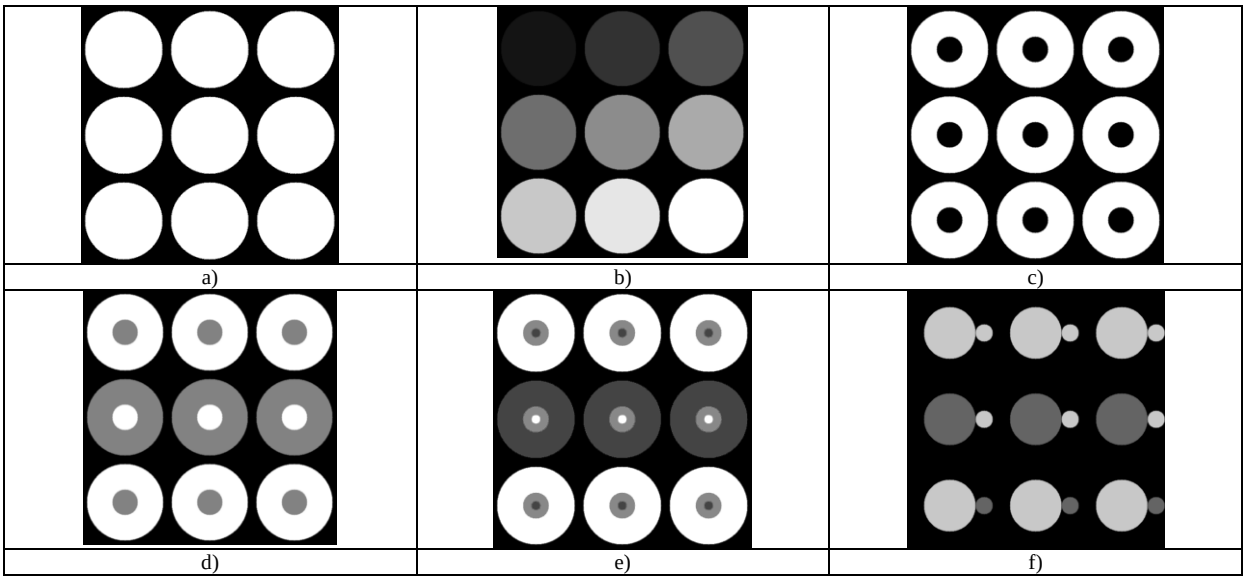

Fig. 1. Test AFM-images: a) AFM-1; b) AFM-2; c) AFM-3; d) AFM-4; e) AFM-5; f) AFM-6

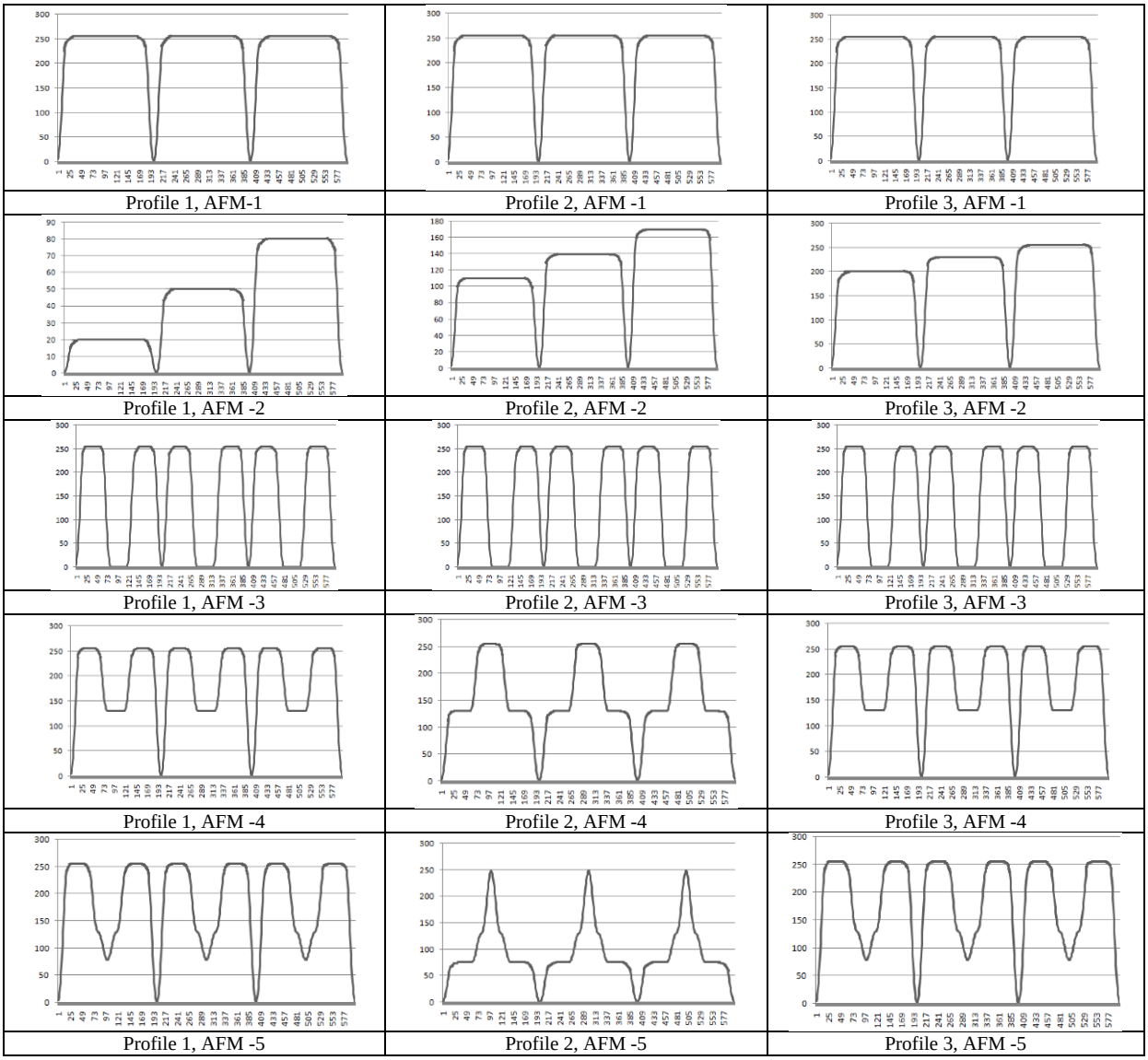

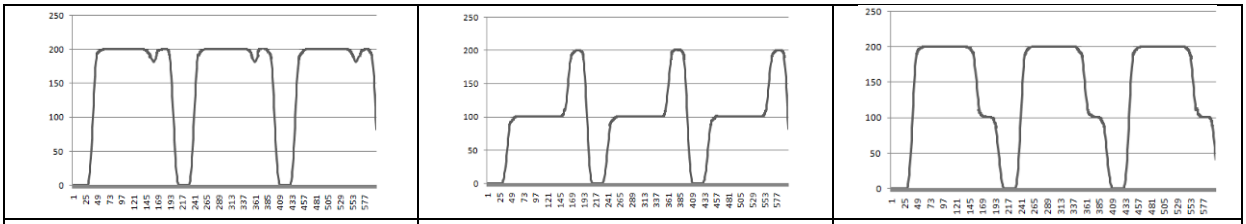

Profile 1, AFM -6	Profile 2, AFM -6	Profile 3, AFM -6

Fig. 2. Profiles of brightness of test AFM-images.

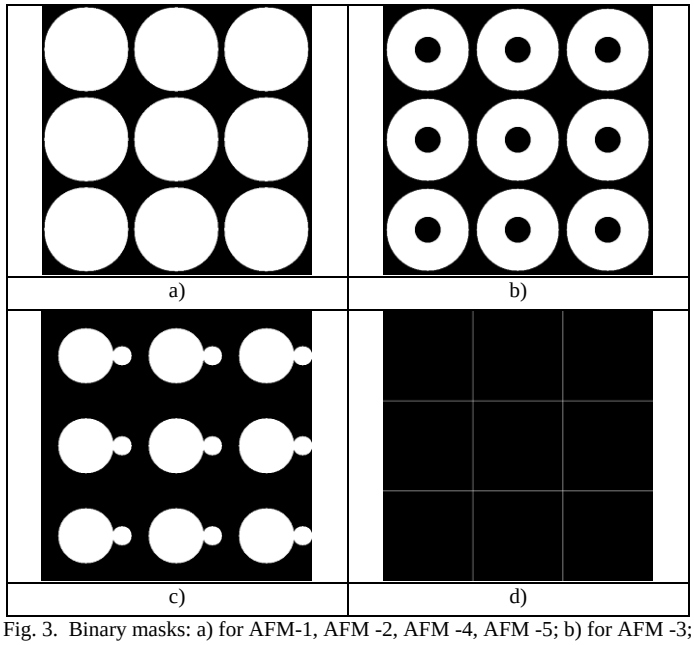

a)	b)
c)	d)

Fig. 3. Binary masks: a) for AFM-1, AFM -2, AFM -4, AFM -5; b) for AFM -3;
c) for AFM -6 with incomplete segmentation; d) for AFM -1 – AFM -6 with complete segmentation

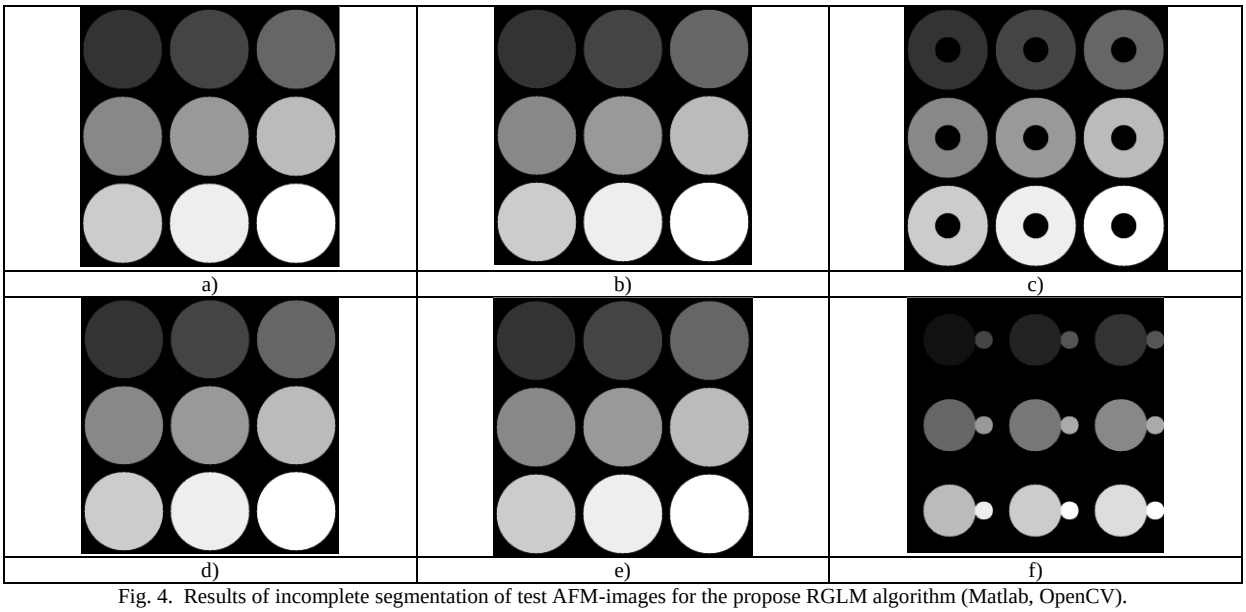

a)	b)	c)
d)	e)	f)

Fig. 4. Results of incomplete segmentation of test AFM-images for the propose RGLM algorithm (Matlab, OpenCV).

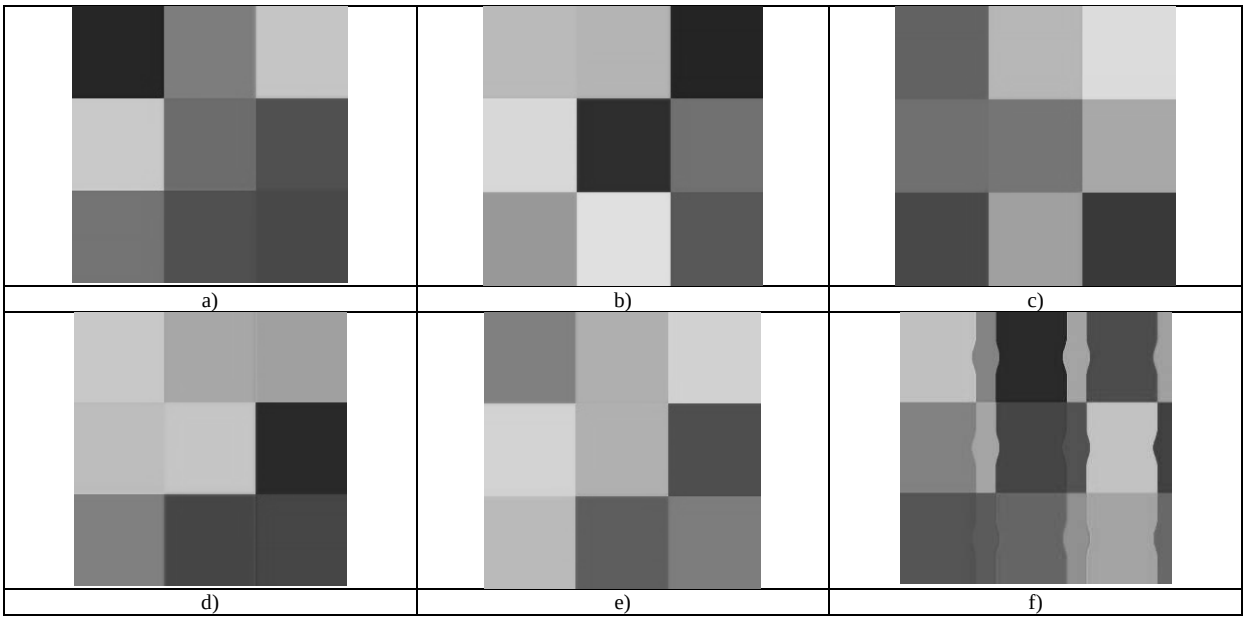

Fig. 5. Results of complete segmentation of test AFM-images for the proposed RGLM algorithm (Matlab, OpenCV).

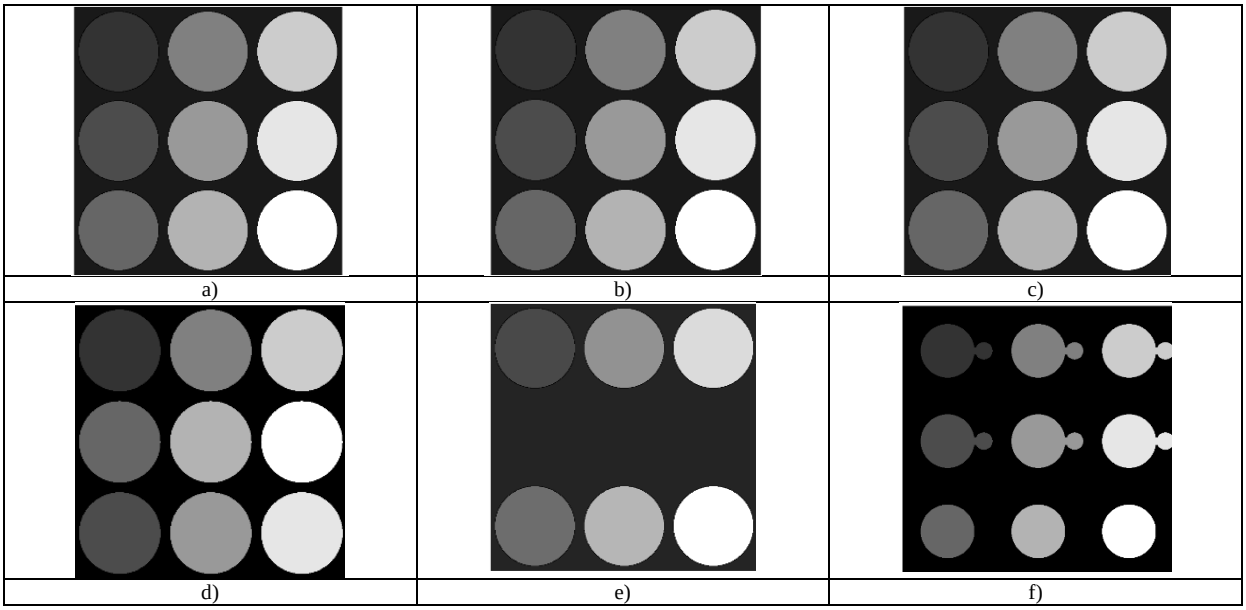

Fig. 6. Results of incomplete segmentation of test AFM-images for MWA algorithm of the marker watershed with automatic marker placement (Matlab).

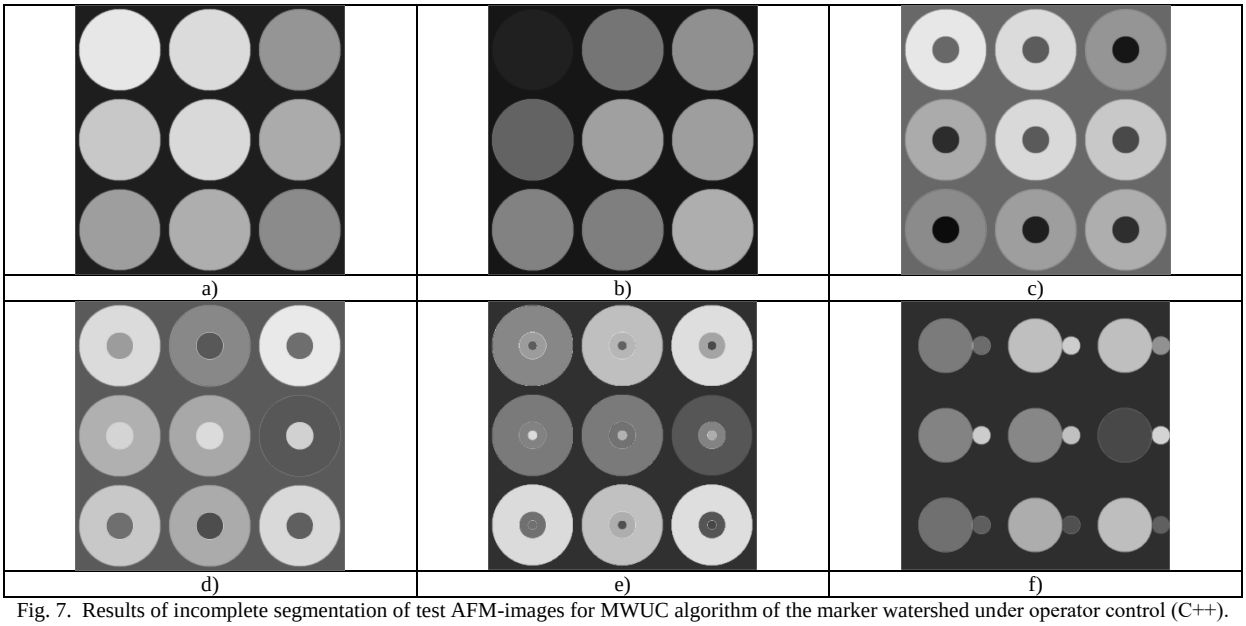

Fig. 7. Results of incomplete segmentation of test AFM-images for MWUC algorithm of the marker watershed under operator control (C++).

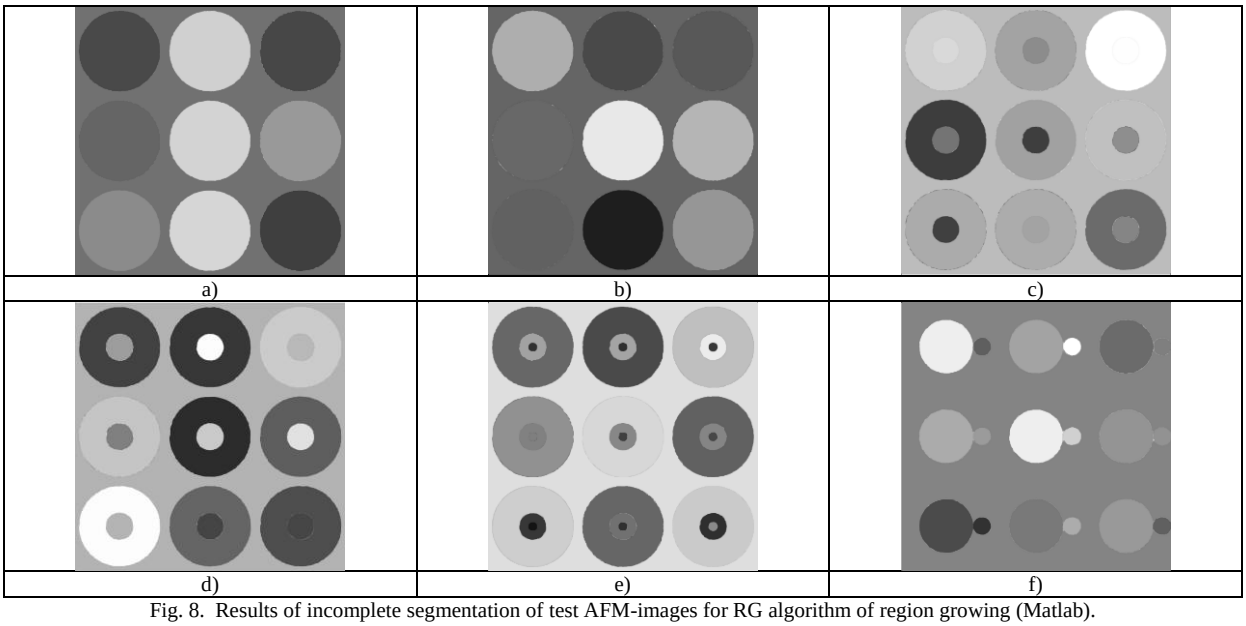

Fig. 8. Results of incomplete segmentation of test AFM-images for RG algorithm of region growing (Matlab).

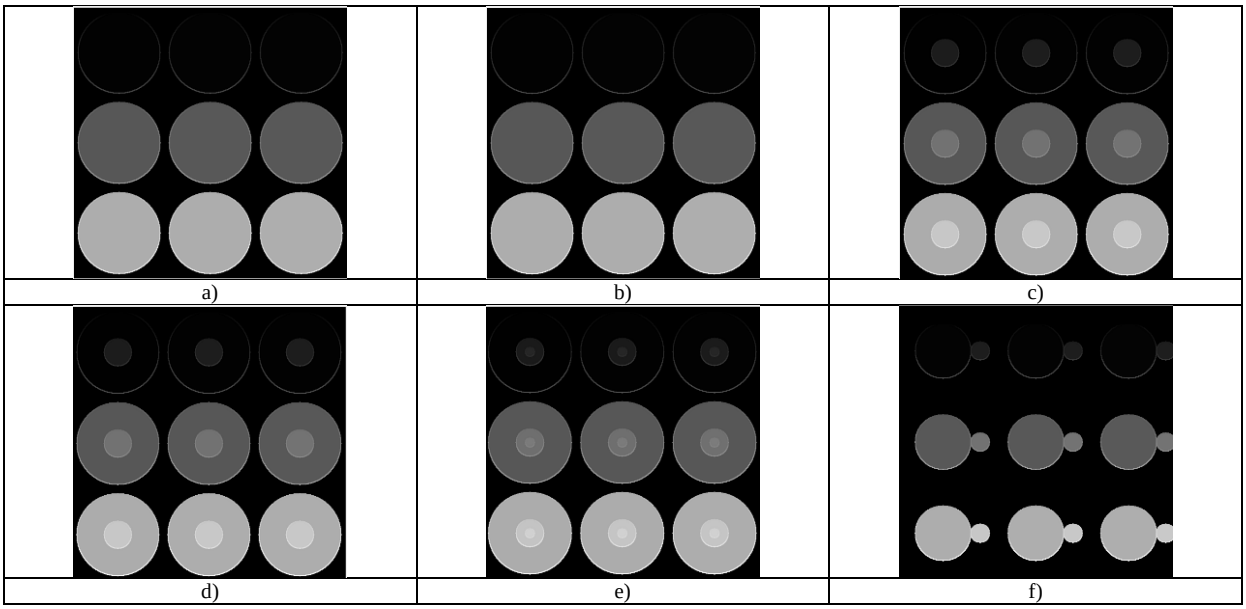

Fig. 9. Results of incomplete segmentation of test AFM-images for RG algorithm of region growing (C++).

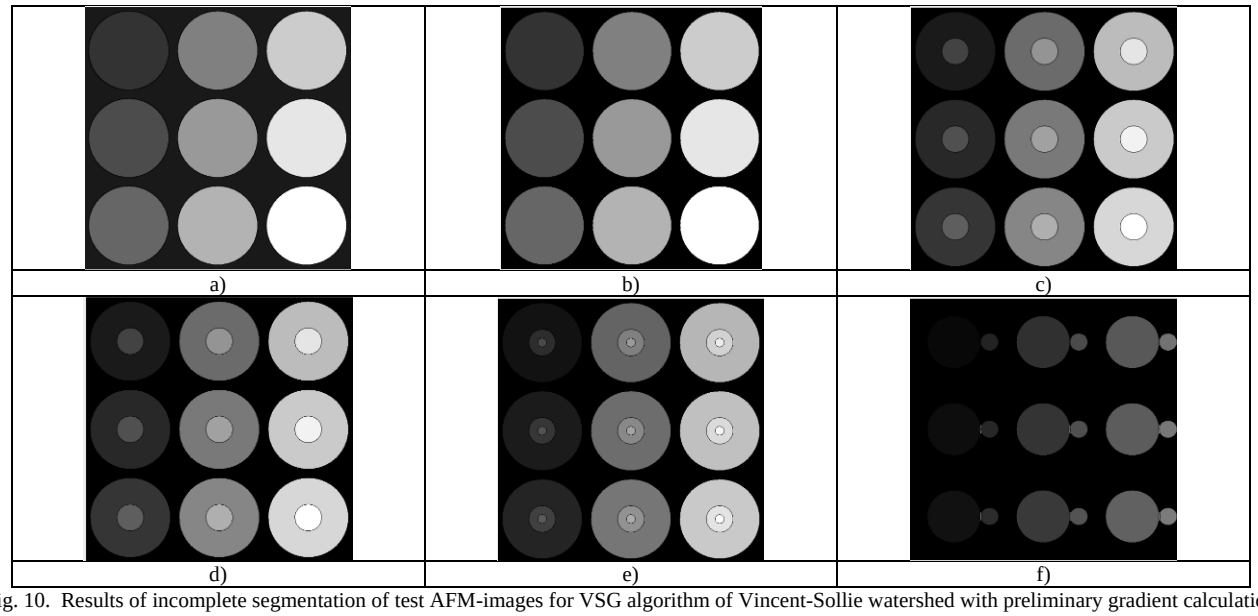

Fig. 10. Results of incomplete segmentation of test AFM-images for VSG algorithm of Vincent-Sollie watershed with preliminary gradient calculation (Matlab).

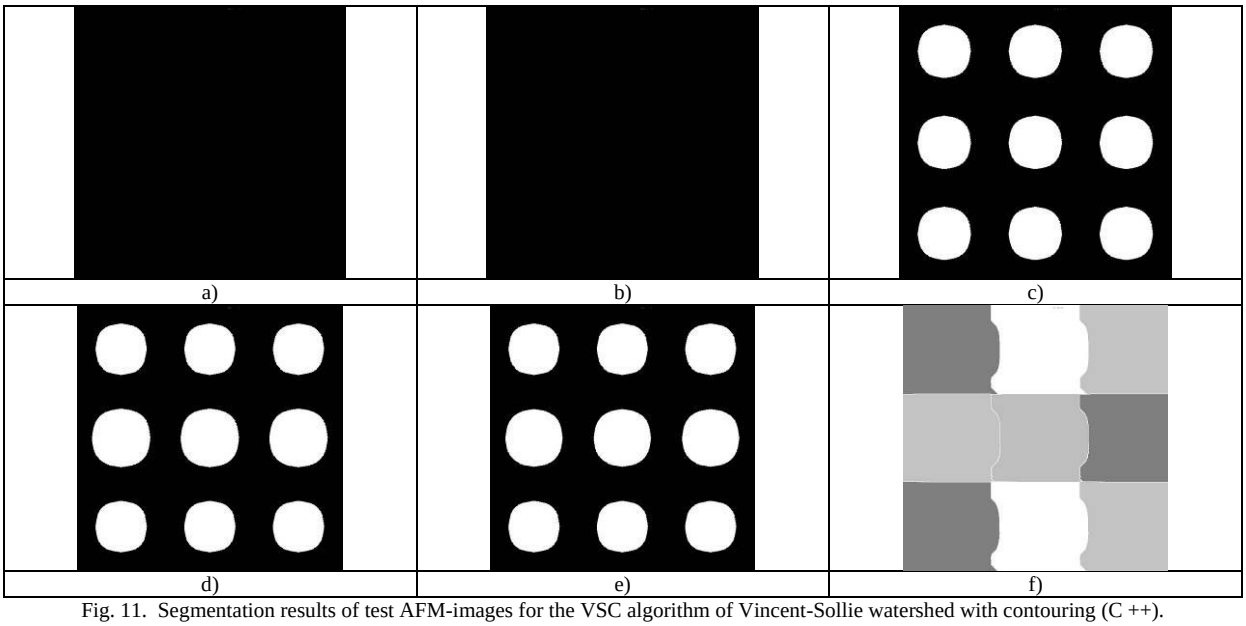

Fig. 11. Segmentation results of test AFM-images for the VSC algorithm of Vincent-Sollie watershed with contouring (C ++).

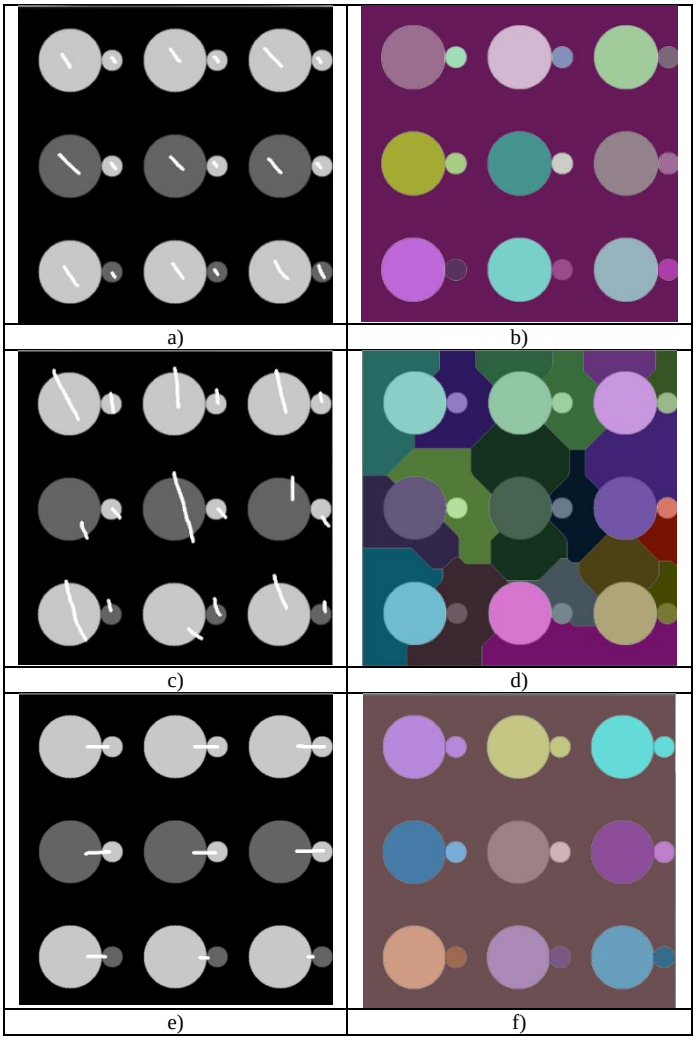

Fig. 12. Segmentation of test AFM-images using a marker watershed under operator control:
a, c, e – operator marker placement options; b, d, f – segmentation results

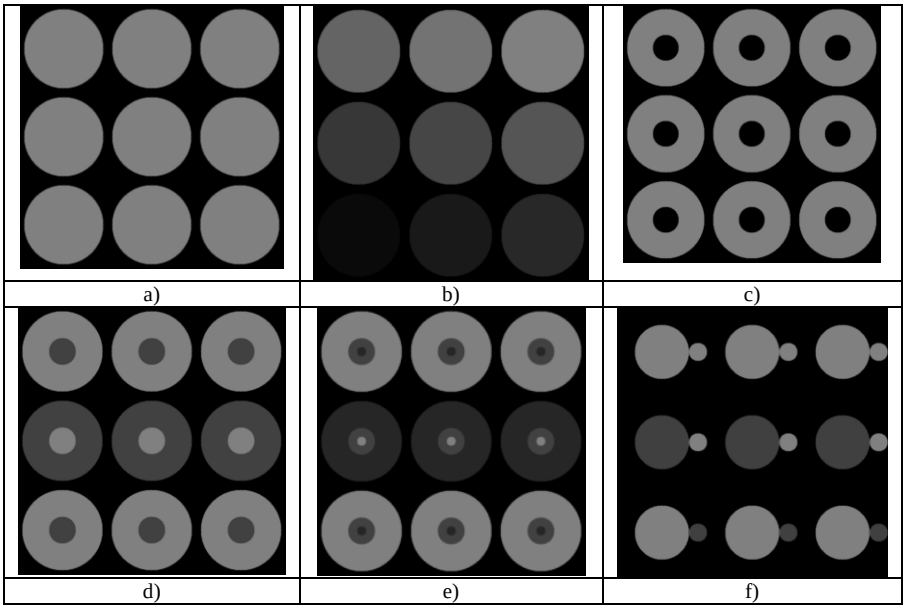

Fig. 13. Segmentation results using Gwyddion program and post-processing.

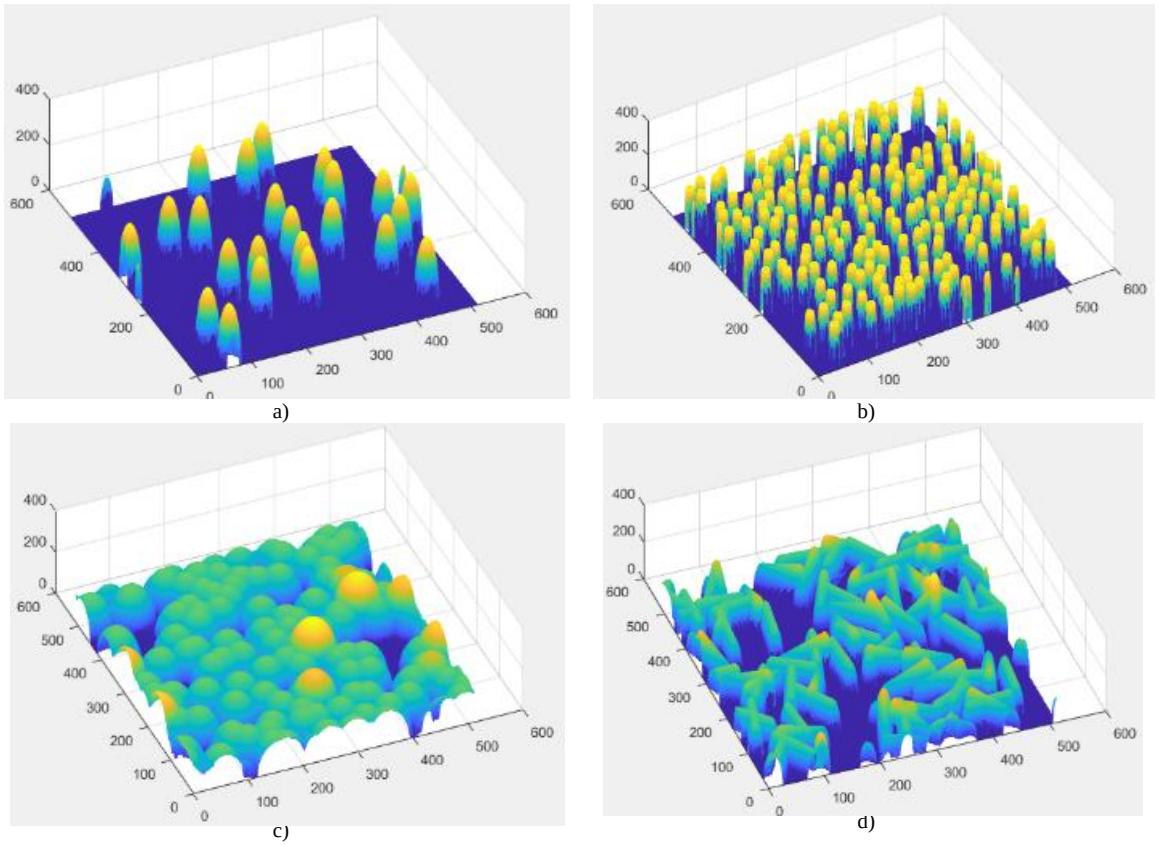

Fig. 14. Three-dimensional models of some test images synthesized in Gwyddion: a, b – the first type of images; c, d – the second type of images;

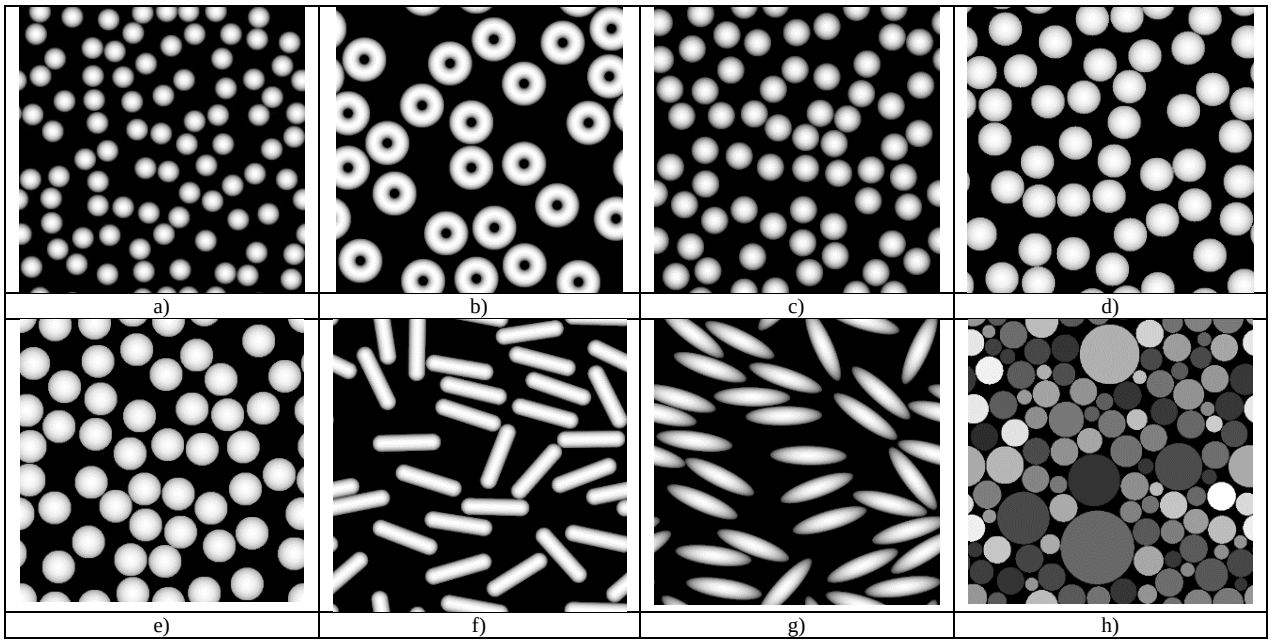

Fig. 15. Test grayscale images of the first type synthesized in Gwyddion: a – AFM_G1-25; b – AFM_G1-45; c – AFM_G1-55; d – AFM_G1-65; e – AFM_G1-80; f – AFM_G1-90; g – AFM_G1-100; h – AFM_G1-105;

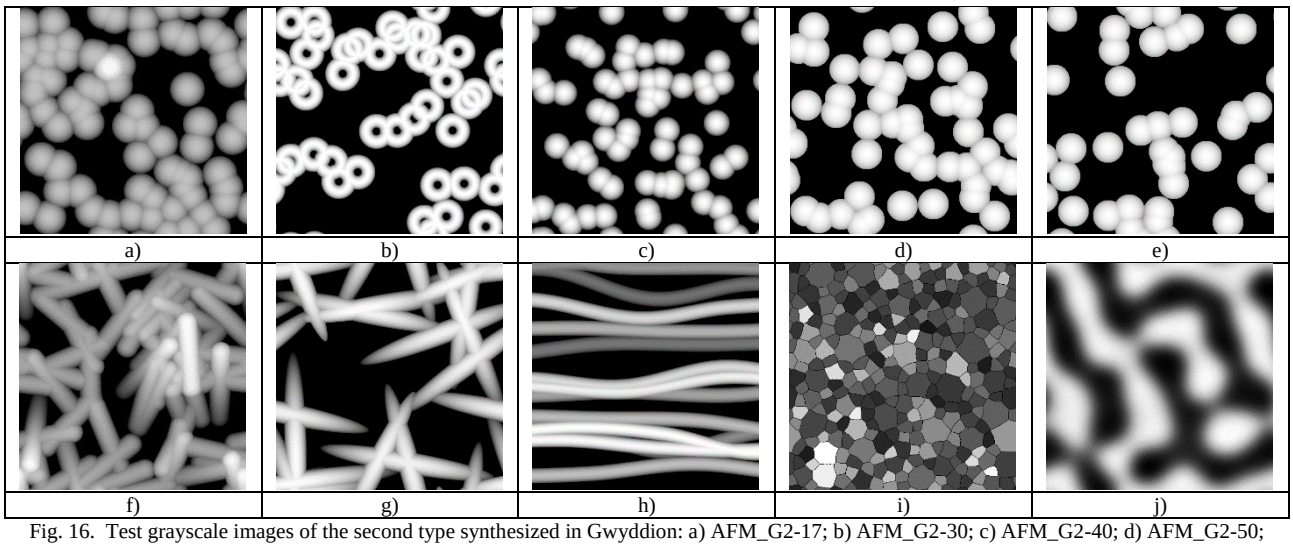

Fig. 16. Test grayscale images of the second type synthesized in Gwyddion: a) AFM_G2-17; b) AFM_G2-30; c) AFM_G2-40; d) AFM_G2-50; e) AFM_G2-60; f) AFM_G2-70; g) AFM_G2-74; h) AFM_G2-80; i) AFM_G2-90; j) AFM_G2-100;

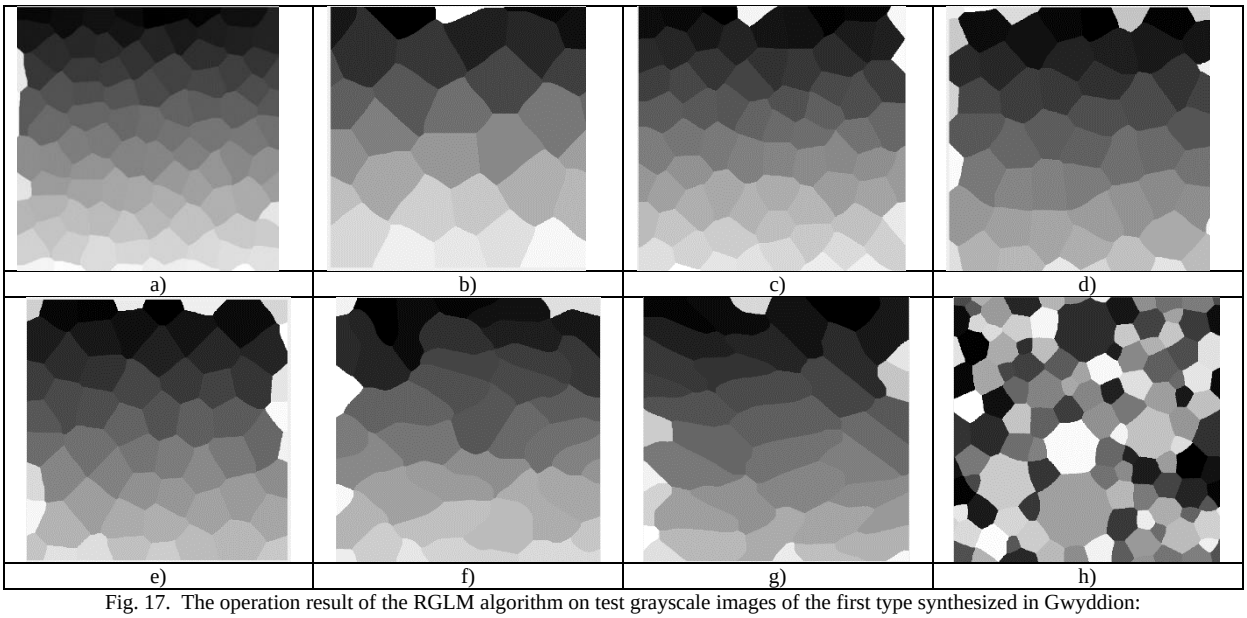

Fig. 17. The operation result of the RGLM algorithm on test grayscale images of the first type synthesized in Gwyddion: a) AFM_G1-25; b) AFM_G1-45; c) AFM_G1-55; d) AFM_G1-65; e) AFM_G1-80; f) AFM_G1-90; g) AFM_G1-100; h) AFM_G1-105;

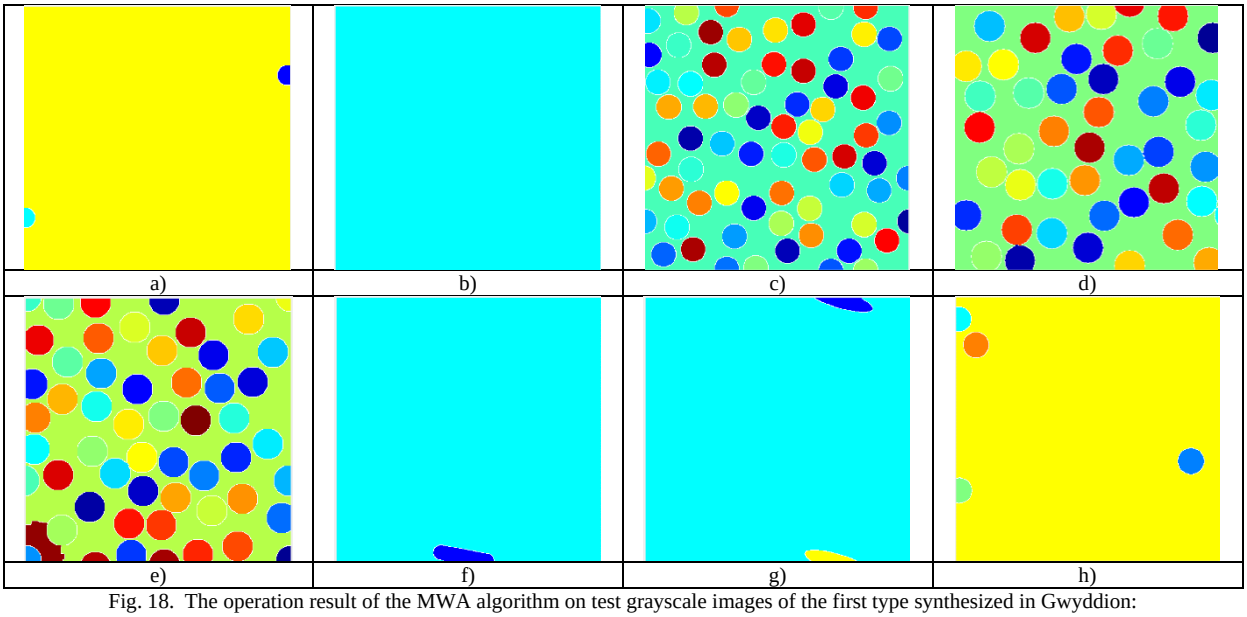

Fig. 18. The operation result of the MWA algorithm on test grayscale images of the first type synthesized in Gwyddion:
a) AFM_G1-25; b) AFM_G1-45; c) AFM_G1-55; d) AFM_G1-65; e) AFM_G1-80; f) AFM_G1-90; g) AFM_G1-100; h) AFM_G1-105;

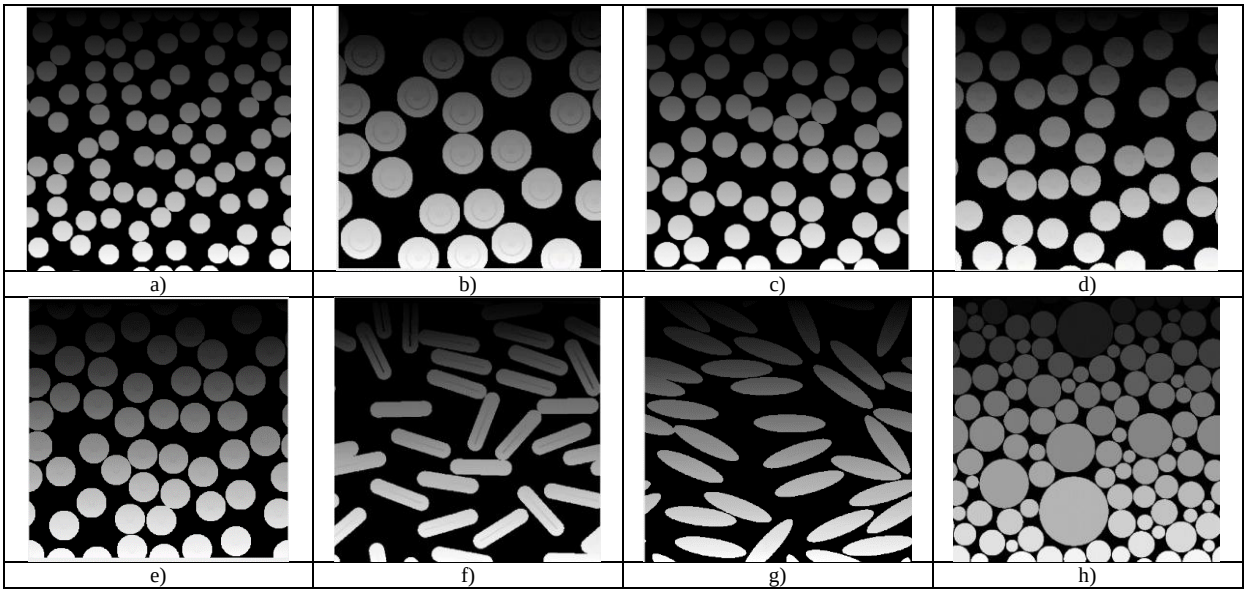

Fig. 19. The operation result of the RG algorithm on test grayscale images of the first type synthesized in Gwyddion:
a) AFM_G1-25; b) AFM_G1-45; c) AFM_G1-55; d) AFM_G1-65; e) AFM_G1-80; f) AFM_G1-90; g) AFM_G1-100; h) AFM_G1-105;

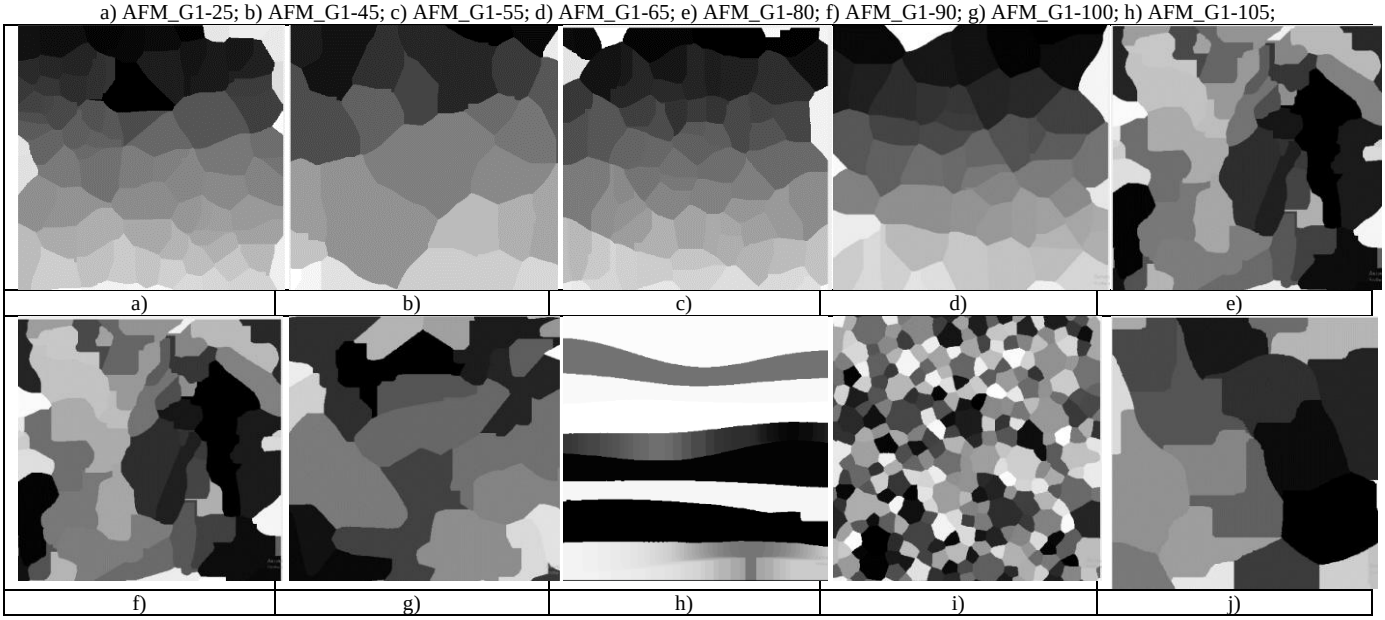

Fig. 20. The operation result of the RGLM algorithm on test grayscale images of the second type synthesized in Gwyddion: a) AFM_G2-17; b) AFM_G2-30; c) AFM_G2-40; d) AFM_G2-50; e) AFM_G2-60; f) AFM_G2-70; g) AFM_G2-74; h) AFM_G2-80; i) AFM_G2-90; j) AFM_G2-100;

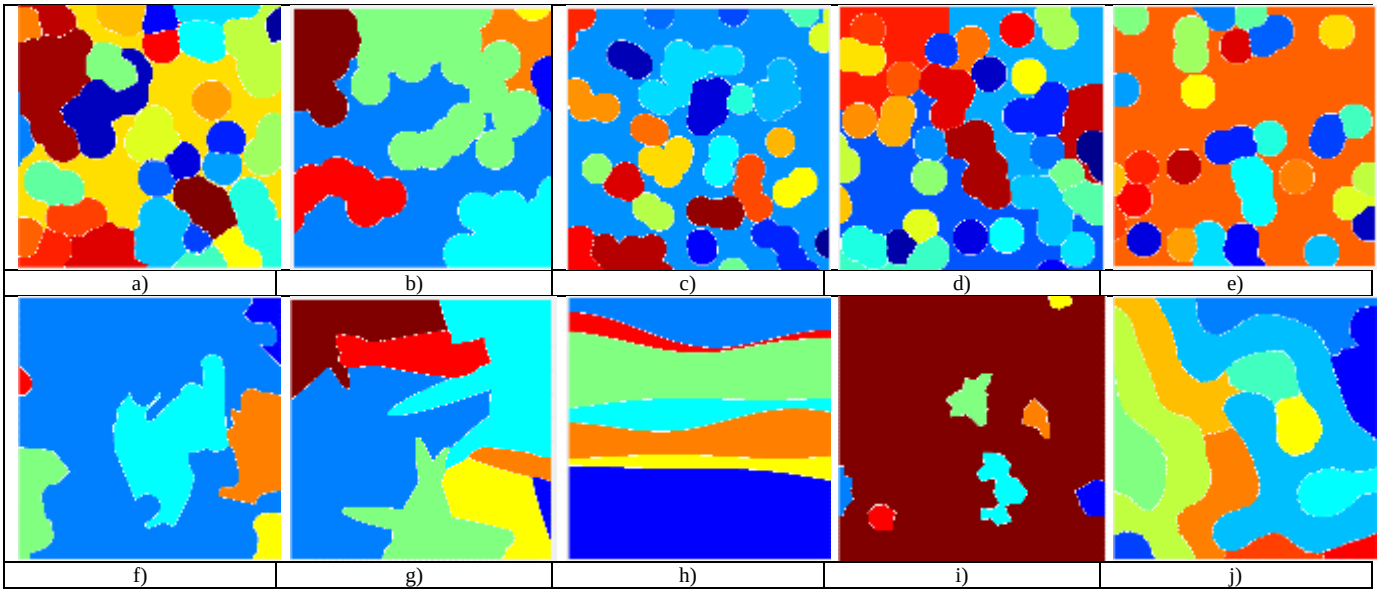

Fig. 21. The operation result of the MWA algorithm on test grayscale images of the second type synthesized in Gwyddion: a) AFM_G2-17; b) AFM_G2-30; c) AFM_G2-40; d) AFM_G2-50; e) AFM_G2-60; f) AFM_G2-70; g) AFM_G2-74; h) AFM_G2-80; i) AFM_G2-90; j) AFM_G2-100;

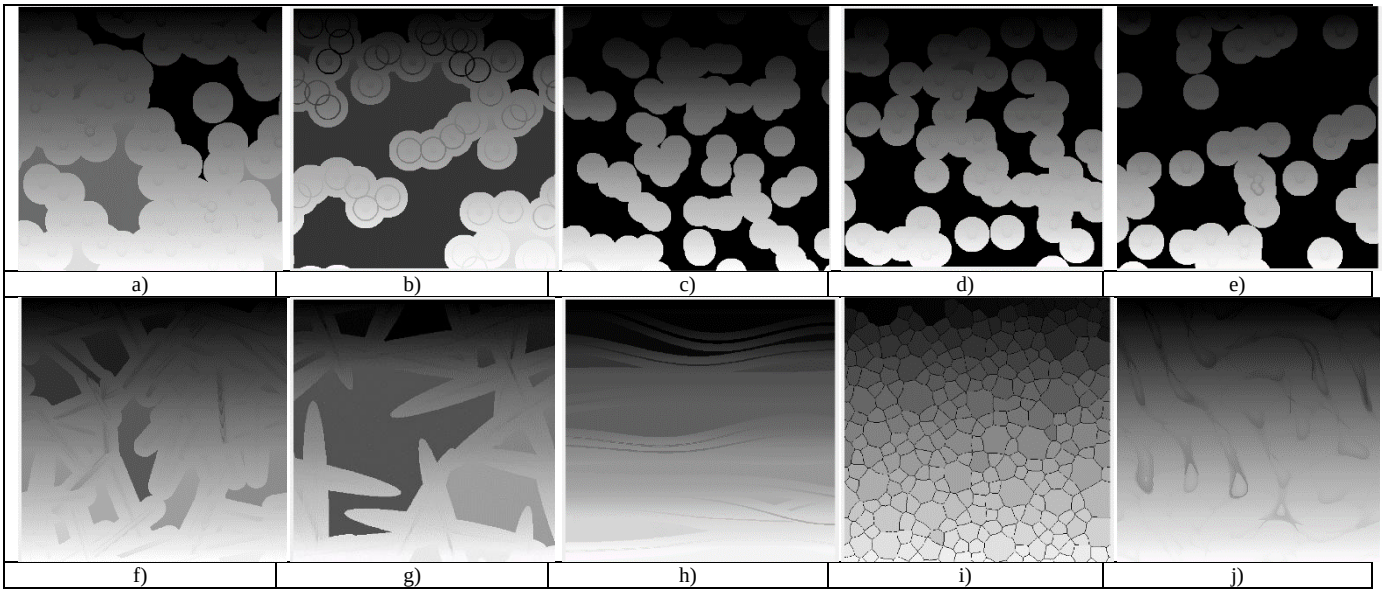

Fig. 22. The operation result of the RG algorithm on test grayscale images of the second type synthesized in Gwyddion: a) AFM_G2-17; b) AFM_G2-30; c) AFM_G2-40; d) AFM_G2-50; e) AFM_G2-60; f) AFM_G2-70; g) AFM_G2-74; h) AFM_G2-80; i) AFM_G2-90; j) AFM_G2-100;

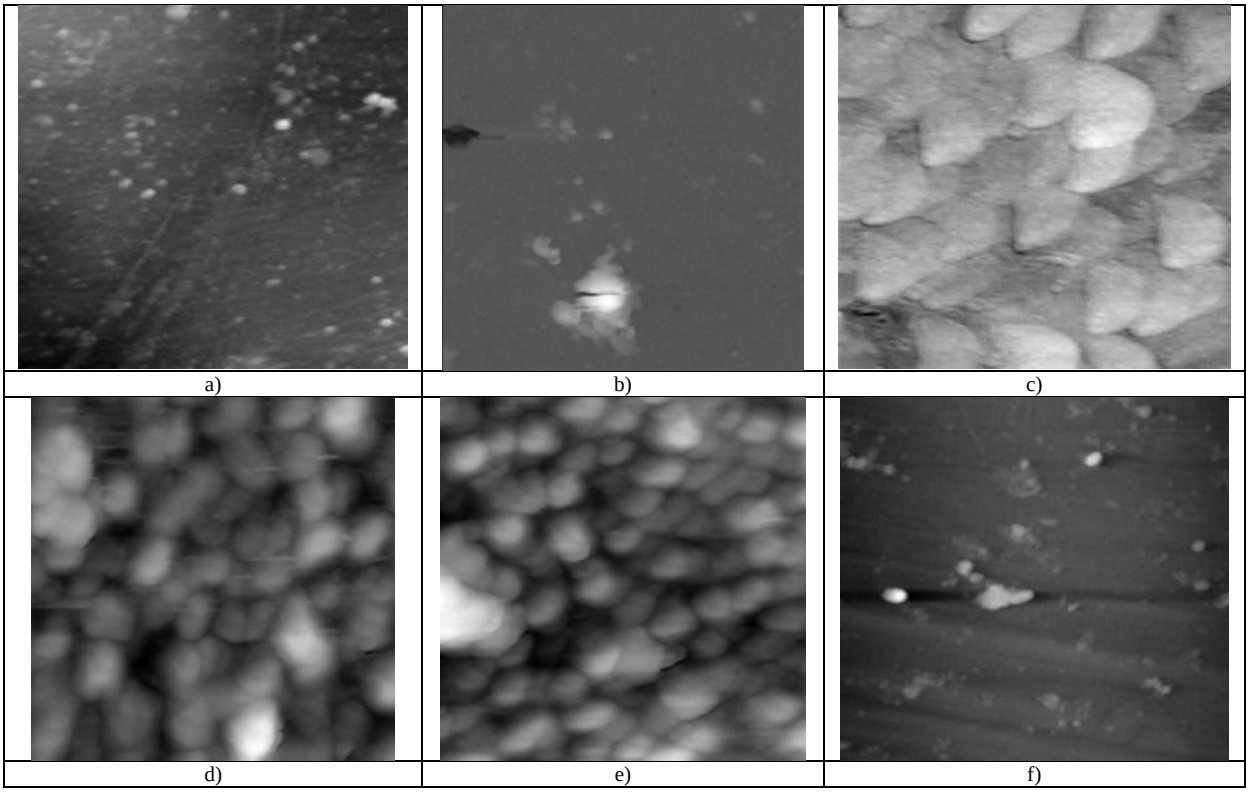

Fig. 23. Original AFM-images in the topography mode: a) polymer surface, scan field size 20 × 20 μm; b) glass surface with defects, scan field size 20 × 20 μm; c) AlSiN nanocrystalline coating surface, is made by blunted probe, scan field size 2 × 2 μm; d) AlSiN nanocrystalline coating surface, made by a new probe, first scan, scan field size 2 ×2 μm; e) AlSiN nanocrystalline coating surface, made by a modified probe, fourth scan, scan field size 2 × 2 μm; f) polymer surface with wave relief, scan field size 20 × 20 μm.

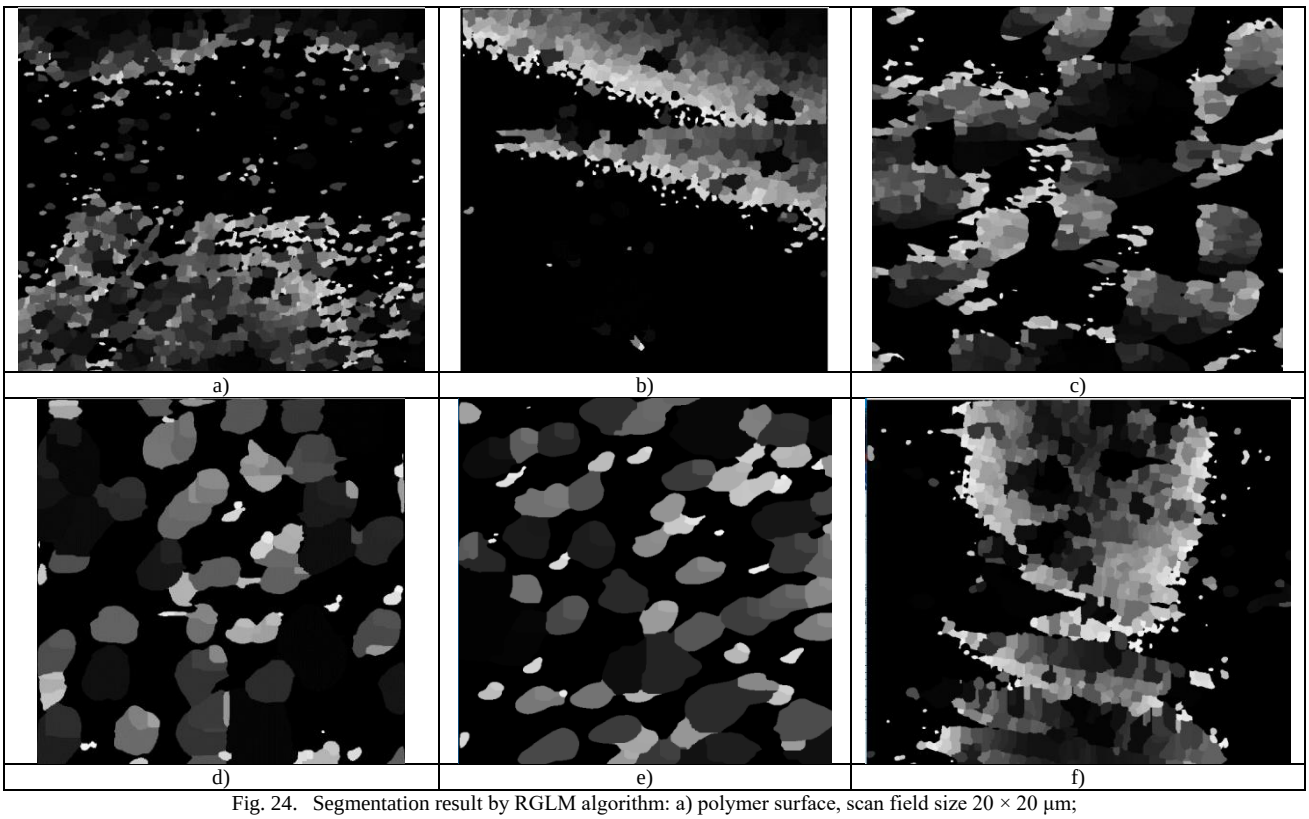

Fig. 24. Segmentation result by RGLM algorithm: a) polymer surface, scan field size 20 × 20 μm; b) glass surface with defects, scan field size 20 × 20 μm; c) AlSiN nanocrystalline coating surface is made by blunted probe, scan field size 2 × 2 μm; d) AlSiN nanocrystalline coating surface, made by a new probe, first scan, scan field size 2 × 2 μm; e) AlSiN nanocrystalline coating surface, made by a modified probe, fourth scan, scan field size 2 × 2 μm; f) polymer surface with wave relief, scan field size 20 × 20 μm.

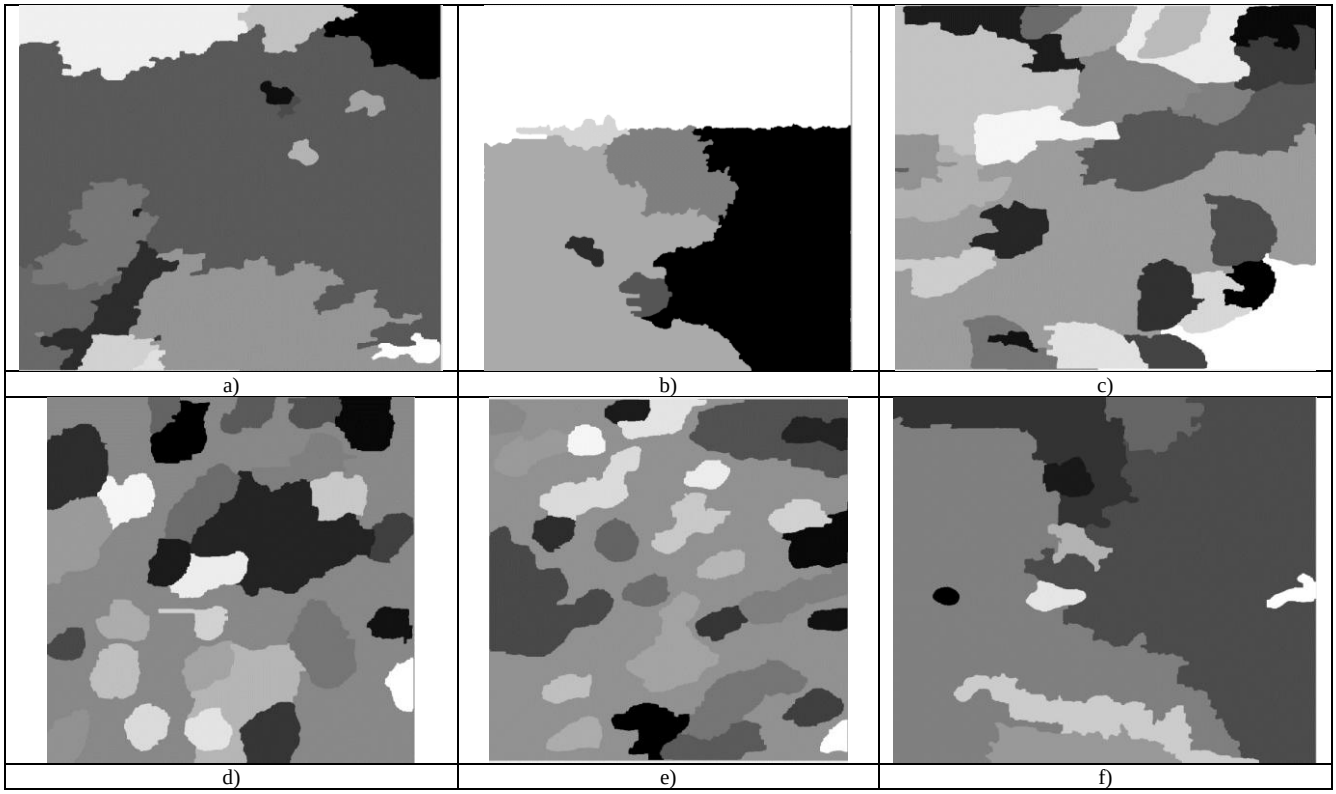

Fig. 25. Segmentation result by MWA algorithm: a) polymer surface, scan field size 20 × 20 μm;
b) glass surface with defects, scan field size 20 × 20 μm; c) AlSiN nanocrystalline coating surface is made by blunted probe, scan field size 2 × 2 μm;
d) AlSiN nanocrystalline coating surface, made by a new probe, first scan, scan field size 2 × 2 μm; e) AlSiN nanocrystalline coating surface, made by a modified probe, fourth scan, scan field size 2 × 2 μm; f) polymer surface with wave relief, scan field size 20 × 20 μm.

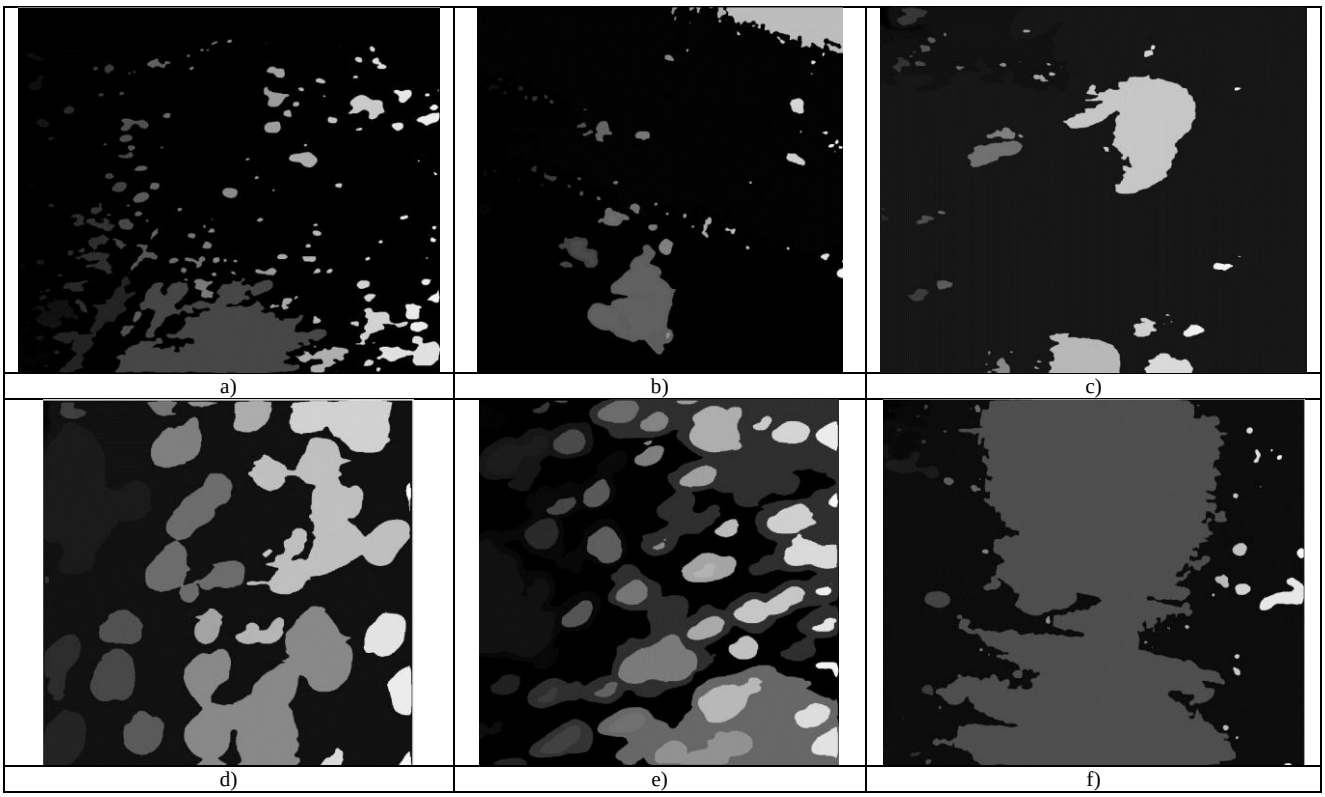

Fig. 26. Segmentation result by VSC algorithm: a) polymer surface, scan field size 20 × 20 μm;
b) glass surface with defects, scan field size 20 × 20 μm; c) AlSiN nanocrystalline coating surface is made by blunted probe, scanning field size 2 × 2 μm;
d) AlSiN nanocrystalline coating surface made by a new probe, first scan, scan field size 2 × 2 μm; e) AlSiN nanocrystalline coating surface made by a modified probe, fourth scan, scan field size 2 × 2 μm; f) polymer surface with wave relief, scan field size 20 × 20 μm.

REFERENCES

[1] V. V. Uglov, V. M. Anishchik , A. K. Kuleshov , I. Polo, F. Tieri, Z. Peletie, T. A. Kuznetsova ,M. P. Samtsov, S. N. Dub, and M. V. Novitskaja, "Interrelation of surface microstructural state and mechanical characteristics of carbon and metal-carbon coatings formed by plasma-enhanced chemical vacuum deposition," Inorganic Materials, 2003, no. 6, pp. 5–11 (in Russian).

[2] M. Andreyev, V. Anishchik, L. Markova, and T. Kuznetsova, "Ion-beam coatings based on Ni and Cr with ultradispersed diamond – structure and properties," Vacuum, 2005, vol. 78, no. 2–4, pp. 451–454. https://doi.org/10.1016/j.vacuum.2005.01.067

[3] M. N. Starodubtseva, T. G. Kuznetsova, T. A. Kuznetsova, Dzh. K. Ellori, S. N. Cherenkevich, and S. O. Abetkovskaya, "Peculiarities of poikilocytosis induced by reactive nitrogen species action," Problems of Health and Ecology, 2006, vol. 8, no. 2, pp. 117–121 (in Russian).

[4] T. M. Ulyanova, L. V. Titova, S. V. Medichenko, Yu. G. Zonov, T. E. Konstantinova, V. A. Glazunova, A. S. Doroshkevich, and T. A. Kuznetsova, "Investigation of the structure of nanocrystalline refractory oxides by X-ray diffraction, electron microscopy and atomic force microscopy,". Crystallography Reports, 2006, vol. 51, no. 1, pp. 144–149.

[5] S. A. Zhdanok, A. I. Sviridenok, M. I. Ignatovskiy, A. V. Krauklis, T. A. Kuznetsova, S. A. Chizhik, and K. O. Borisevich, "On the properties of a steel modified with carbon nanomaterials," Journal of Engineering Physics and Thermophysics, 2010, vol. 83, no. 1, pp. 1–5. https://doi.org/10.1007/s10891-010-0312-8

[6] L. M. Slepneva, and T. A. Kuznetsova, "Dispersibility and morphology of titanium dioxide hydrosols," Science and Technology, 2012, no. 5, pp. 3–7 (in Russian).

[7] S. A. Chizhik, T. A. Kuznetsova, A. L. Khudoley, A. I. Komarov, V. I. Komarova, and M. S. Vasilenko, "Nanosized substructure of heat-treated high-strength cast iron," Journal of Engineering Physics and Thermophysics, 2013, vol. 86, no. 5, pp. 1008–1019. https://doi.org/10.1007/s10891-013-0922-z

[8] T. A. Kuznetsova, S. A. Chizhik, and A. L. Khudoley, "Deformation structuring of aluminum films during microindentation," The Journal of Surface Investigation. X-ray, Synchrotron and Neutron Techniques, 2014, no. 12, pp. 46–56 (in Russian).

[9] L. M. Slepneva, T. A. Kuznetsova, V. A. Gorbunova, G. E. Slepnev, and S. A. Chizhik, "Production of titanium dioxide powder by solvolysis method and estimation of its dispersion," Proceedings of the National Academy of Sciences of Belarus. Physical-technical series, 2015, no. 1, pp. 10–15 (in Russian).

[10] T. Kuznetsova, T. Zubar, S. Chizhik, A. Gilewicz, O. Lupicka, and B. Warcholinski, "Surface microstructure of Mo(C)N coatings investigated by AFM," Journal of Materials Engineering and Performance, 2016, vol. 25, no. 12, pp. 5450–5459. https://doi.org/10.1007/s11665-016-2390-z

[11] N. A. Geisse, "AFM and Combined Optical Techniques," Materials Today, 2011, vol. 12, no. 7–8, pp. 40–45.

[12] Ahmad Wahyu Rosyadi, and Nanik Suciati, "Image Segmentation Using Transition Region and K-Means Clustering," IAENG International Journal of Computer Science, vol. 47, no.1, pp. 47–55, 2020.

[13] Qingrui Zhang, Mingqiang Yang, Kidiyo Kpalma, Qinghe Zheng, and Xinxin Zhang, "Segmentation of Hand Posture against Complex Backgrounds Based on Saliency and Skin Colour Detection," IAENG International Journal of Computer Science, vol. 45, no.3, pp. 435–444, 2018.

[14] N. Mohd Saad, N. S. M. Noor, A.R. Abdullah, Sobri Muda, A. F. Muda, and Haslinda Musa, "Segmentation and Classification Analysis Techniques for Stroke based on Diffusion-Weighted Images," IAENG International Journal of Computer Science, vol. 44, no.3, pp. 388–395, 2017.

[15] Yoshitomo Akimoto, Takenori Sakumura, and Toshinari Kamakura, "Testing for Uniformity of Line Segments," IAENG International Journal of Computer Science, vol. 43, no.2, pp. 192–197, 2016.

[16] P. Eaton and P. West, Atomic Force Microscopy, Oxford University Press, 2010, p. 257.

[17] W. K. Pratt, Digital Image Processing, 3rd edition, Los Altos, California: Jonh Willey & Sons, Inc., 2001, p. 738.

[18] R. C. Gonzalez and R. E. Woods, Digital Image Processing, Pearson Education, 2008, p. 954.

[19] S. Beucher and C. Lantuéjoul, "Use of watersheds in contour detection," Proc. International Workshop on Image Processing, Real-Time Edge and Motion Detection/Estimation, Rennes, 1979. http://www.cmm.mines-paristech.fr/~beucher/publi/watershed.pdf

[20] L. Vincent and P. Sollie, "Watershed in digital spaces: an efficient algorithm based on immersion simulation," IEEE Transactions on Pattern Analysis and Machine Intelligence, vol. 13, pp. 583–598, 1991.

[21] P. T. Jackway, "Gradient watersheds in morphological scale space," IEEE Transactions on Image Processing, vol. 5, no. 6, pp. 913–921, 1999.

[22] J. Weickert, "Efficient image segmentation using partial differential equations and morphology," Pattern Recognition, vol. 34, pp. 1813–1824, 2001.

[23] C. R. Jung and J. Scharcanski, "Robust watershed segmentation using wavelets," Image and Vision Computing, vol. 23, pp. 661–669, 2005.

[24] "Marker-controlled watershed segmentation," [Electronic resource], MathWork, Mode of access: https://www.mathworks.com/help/images/examples/marker-controlled-watershed-segmentation.html – Date of access: 02.04.2018

[25] O. M. Almiyahi, V. Yu. Tsviatkou, and V. K. Kanapelka, "Image segmentationn based on the wave region growing," Doklady BGUIR, 2016, vol. 3, no. 97, pp. 24–30 (in Russian).

[26] "Watershed segmentation algorithm in OpenCV," [Electronic resource], Github, Mode of access: https://github.com/AlmogDavid/fellowQuad/blob/1d26f32ba44cba0426af6e6c40bcd73e0db6f9ba/opencv/Source.cppl – Date of access: 02.04.2018.

[27] "Region growing algorithm," [Electronic resource], Github, Mode of access: https://github.com/emreozanalkan/RegionGrowingAlgorithm – Date of access : 02.04.2018.

[28] "Watershed," [Electronic resource], MathWork, Mode of access: https://www.mathworks.com/help/images/ref/watershed.html?s_tid=srchtitle – Date of access: 02.04.2018.

[29] "Watershed," [Electronic resource], Github, Mode of access: https://github.com/keke2014/Watershed – Date of access: 02.04.2018.

[30] "Gwyddion," [Electronic resource], Mode of access: http://gwyddion.net – Date of access: 02.04.2018.

Oday Jasim Mohammed Al-Furaiji is a lecturer at the Department of Computer Science, Shatt Al-Arab University College, Basra, Iraq.
Ph. D. Degree from Belarusian State University of Informatics and Radioelectronics (BSUIR), Minsk, Belarus Specialty: Telecommunication Systems, Networks and Devices
Email: odaymohammed@mail.ru

Violetta Viktorovna Rabtsevich – assistant of the department of Infocommunication Technologies of Belarusian State University of Informatics and Radioelectronics
Minsk, Belarus
rabcevichv@gmail. com

Viktar Yurevich Tsviatkou – Doctor of Engineering, associate professor, head of department of infocommunication technologies of Belarusian State University of Informatics and Radioelectronics (BSUIR), Minsk, Belarus. Specialty: Telecommunication Systems, Networks and Devices
Email: vtsvet@bsuir.by

Tatiana Anatolyevna Kuznetsova is Deputy of Head of the Laboratory of Nanoprocesses and Technologies
A.V. Luikov Heat and Mass Transfer Institute of the National Academy of Sciences, Minsk, Belarus
kuzn06@mail.ru

Sergey Antonovich Chizhik is First Deputy Chairman of the Presidium of the National Academy of Sciences of Belarus
Chief Researcher A.V. Luikov Heat and Mass Transfer Institute of the National Academy of Sciences
Minsk, Belarus
chizhik_sa@tut.by